

# III. ÖRÆFAJÖKULL VOLCANO: ERUPTION MELTING SCENARIOS

Magnús T. Guðmundsson \*, Þórdís Högnadóttir \*, Eyjólfur Magnússon \*

\* *Nordic Volcanological Centre, Institute of Earth Sciences, University of Iceland*

## 1. Introduction

Observations of recent volcanic unrest demonstrate that melting of ice in eruptions within glaciers can be extremely fast. The best documented cases have occurred in the last quarter of a century in Grímsvötn, Gjálp, Eyjafjallajökull and Redoubt in Alaska (e.g. Guðmundsson *et al.*, 1997, 2004; Guðmundsson, 2005; Magnússon *et al.*, 2012a; Waythomas *et al.*, 2013) and some earlier events such as the Katla 1918 eruption (Tómasson, 1996; Björnsson, 2003) and the eruptions of Mount St. Helens in 1980–1983 (Pierson, 1999), Nevado del Ruiz in 1985 (Pierson *et al.*, 1990) and Redoubt in 1989–90 (Dorava and Meyer, 1994; Trabant *et al.*, 1994). For eruptions observed in Iceland, the highest rates of heat transfer and melting occur in the early, fully subglacial phases of explosive eruptions where the magma is fragmented into glass particles, typically in the size range 0.01–1 mm (e.g. Guðmundsson, 2003). More gradual melting is expected to occur when heat transfer takes place largely by free convection of water above rapidly cooled lava under ice (e.g. Höskuldsson and Sparks, 1997; Guðmundsson, 2003; Woodcock *et al.*, 2012, 2014). Thus, because of their greater potential to melt large amounts of ice in a short period of time, eruptions where fragmentation is dominant are more dangerous. The analysis presented here is therefore mostly concentrated on eruptions dominated by fragmentation and their consequences.

The purpose of the present work is to estimate the potential hazard due to jökulhlaups

associated with volcanic activity in Öräfajökull. The approach is therefore to consider what can be defined as realistic worst case scenarios. This needs to be kept in mind when considering the results. The scenarios with the highest probability are less extreme. Three types of eruptions/events are considered. (1) Eruptions within the caldera of Öräfajökull (thick ice), (2) eruptions on the flanks (thin ice), and (3) pyroclastic density currents (PDCs). The values of various parameters used in calculations and definitions of terms are listed in Table III-1. In this chapter a short overview of the area being considered is given in Section 2 while the magnitudes of eruptions that occur in Iceland are reviewed briefly in Section 3. In Section 4, calorimetric considerations on the various types of volcanic events are presented and empirical data used to constrain efficiencies of processes. The jökulhlaups, their entrainment of volcanic material and the onset times are considered in Section 5. It is assumed that a flood breaks through the ice and starts to cascade downslope mostly on the surface and along the margins of outlet glaciers where ice on the slopes is shallow as on Öräfajökull. This behaviour was for example observed in Eyjafjallajökull in 2010 (Magnússon *et al.*, 2012a). The propagation of the flood once it has reached the upper parts of the outlets is not considered further here since it is dealt with in Chapter IV (Helgadóttir *et al.*, 2015). The results for the various catchments and outlet glaciers for the three types of events considered are presented in Section 6.

Table III-1: List of symbols, abbreviations and numerical values of parameters.

Symbol	definition	Unit
<i>PDC</i>	Pyroclastic density current	-
<i>MER</i>	Mass eruption rate	kg/s
<i>EOT</i>	Eruption onset time	min
<i>STT</i>	Subglacial transport time	min
<i>FTT</i>	Flank transit time	min
$\frac{dE}{dt}$	Rate of heat transfer / energy flux	W
$E_p$	Energy available to melt snow and ice in a PDC	J
$f$	Efficiency of heat transfer (0–100%, in reality $f_{max} \sim 80\text{--}90\%$ )	Dimensionless
$\chi$	Fraction of tephra entrained in phoenix cloud during PDC formation	Dimensionless
$\xi$	Fraction of PDC flowing over a particular catchment	Dimensionless
$Q_m$	Volumetric flow rate of magma	m <sup>3</sup> /s
$\dot{M}_m$	Mass eruption rate	kg/s
$\dot{m}$	Mass eruption rate per unit length of volcanic fissure	(kg/s)/m
$\dot{M}_p$	Mass generation rate of pyroclastic material at eruption site (usually equal to mass eruption rate)	kg/s
$\dot{M}_w$	Mass generation rate of meltwater at eruption site	kg/s
$Q_1, Q_2,$ $Q_w$	Rate of liquid water generation by ice melting	m <sup>3</sup> /s
$Q_T$	Discharge of jökulhlaup (liquid water + entrained ice and pyroclasts)	m <sup>3</sup> /s
$\rho_m$	Magma density	kg/m <sup>3</sup>
$\rho_g$	Tephra	kg/m <sup>3</sup>
$\rho_i$	Density of ice	kg/m <sup>3</sup>
$\rho_w$	Density of liquid water	kg/m <sup>3</sup>
$T_i, T_f, \Delta T$	Temperature, i: initial, f: final, $\Delta T$ : temperature difference	°C
$T_e$	Emplacement temperature of pyroclastic density current	°C
$T_0$	Ambient air/snow temperature ( $\sim 0^\circ\text{C}$ )	°C
$L_i$	Latent heat of solidification of ice, $L_i = 3.34 \times 10^5$ J/kg	J/kg
$C_g$	Specific heat capacity of fresh volcanic glass	J/(kg °C)
$C_p$	Specific heat capacity of pyroclastic material in collapse	J/(kg °C)
$l$	Length – used here for volcanic fissure at base of glacier	m
$x$	Length	m
$q$	Rate of meltwater production per unit length of fissure	m <sup>2</sup> /s
$\Delta V_i$	Volume of ice	m <sup>3</sup>
$M_p$	Mass of pyroclastic material	kg
$M_g$	Mass of pyroclasts interacting with glacier/snow in pyroclastic density current	kg

Symbol	definition	Unit
$\tau$	Duration of plume collapse forming pyroclastic density current.	s
$t_{run}$	Period it takes a ground hugging PDC to flow over snow/ice and release heat	s
$\varphi$	Static fluid potential of water flow under ice	Pa
$g$	Acceleration due to gravity $g = 9.82 \text{ m/s}^2$	$\text{m/s}^2$
$z_b$	Height of glacier bed (usually above sea level)	m
$z_s$	Height of glacier surface (usually above sea level)	m

## 2. Öraefajökull and its potential to generate jökulhlaups

The height and overall morphology of Öraefajökull with an ice-filled caldera and ice covered upper slopes makes jökulhlaups an almost inevitable consequence of eruptions on the upper parts of the volcano. The two historical examples of 1362 and 1727 demonstrate this, as shown by Thorarinsson (1958) and Roberts and Gudmundsson (2015; this volume, chapter II). The part of the mountain massif considered here is the presently active volcano south of Svínafellsjökull and Hermannaskarð (Figures III-1 and III-2). The ice-covered part of the volcano has recently been mapped with radio-echo soundings (Magnússon *et al.*, 2012b). For the jökulhlaup hazard, the following water catchment basins were considered:

- i) The southern catchment of Svínafellsjökull:* Only considered here as a potential source of jökulhlaups caused by pyroclastic density currents.
- ii) Virkisjökull-Falljökull:* This includes a section of the caldera and the flanks north of Sandfell. Can be affected by caldera eruptions, flank eruptions and pyroclastic density currents. This also includes Grænafjallsgljúfur, to the south of Falljökull.
- iii) Kotárjökull:* This catchment reaches the caldera rim but is mainly confined to the slopes. Flank eruptions can occur here and the flanks of the catchment can be affected by pyroclastic density currents.

*iv) Rótarfjallshnjúkur-Hnappur and glaciers to the south of these nunataks:* The upper boundary of this segment is the southern caldera rim. Can be affected by flank eruptions and pyroclastic density currents.

*v) Kviárjökull:* This includes a large part of the caldera, the slopes of Kviárjökull and its lower part. Can be affected by caldera eruptions, flank eruptions and pyroclastic density currents.

*vi) Eastern flank of Öraefajökull north of Kviárjökull:* The upper slopes are similar to those on the west side and can be affected by flank eruptions and possibly pyroclastic density currents. However, since the inundation area of jökulhlaups is not inhabited, this segment is not considered in the same way as those on the west and south side.

## 3. Magma discharge in eruptions

Models exist that relate magma flow rate in an explosive eruption with eruption plume height (Sparks *et al.*, 1997; Mastin *et al.*, 2009; Woodhouse *et al.*, 2013; Degruyter and Bonadonna, 2012). These equations, however, are very sensitive to the plume height, the plume height is related to both magma flow rate and wind speed and discrepancies between predicted and observed flow rate may be as much as a factor of 3–4 (Oddsson *et al.*, 2012). These equations are not used here.

In Table III-2 the estimated magma flow rate of several Icelandic eruptions are given

together with known fissure lengths. In most cases the numbers in the table are mean values over some interval during the most powerful phase of the eruption.

However, the peak values may well have been 2–3 times higher in some cases and for the largest ones  $\dot{M}$  may have reached or exceeded  $10^8$  kg/s.

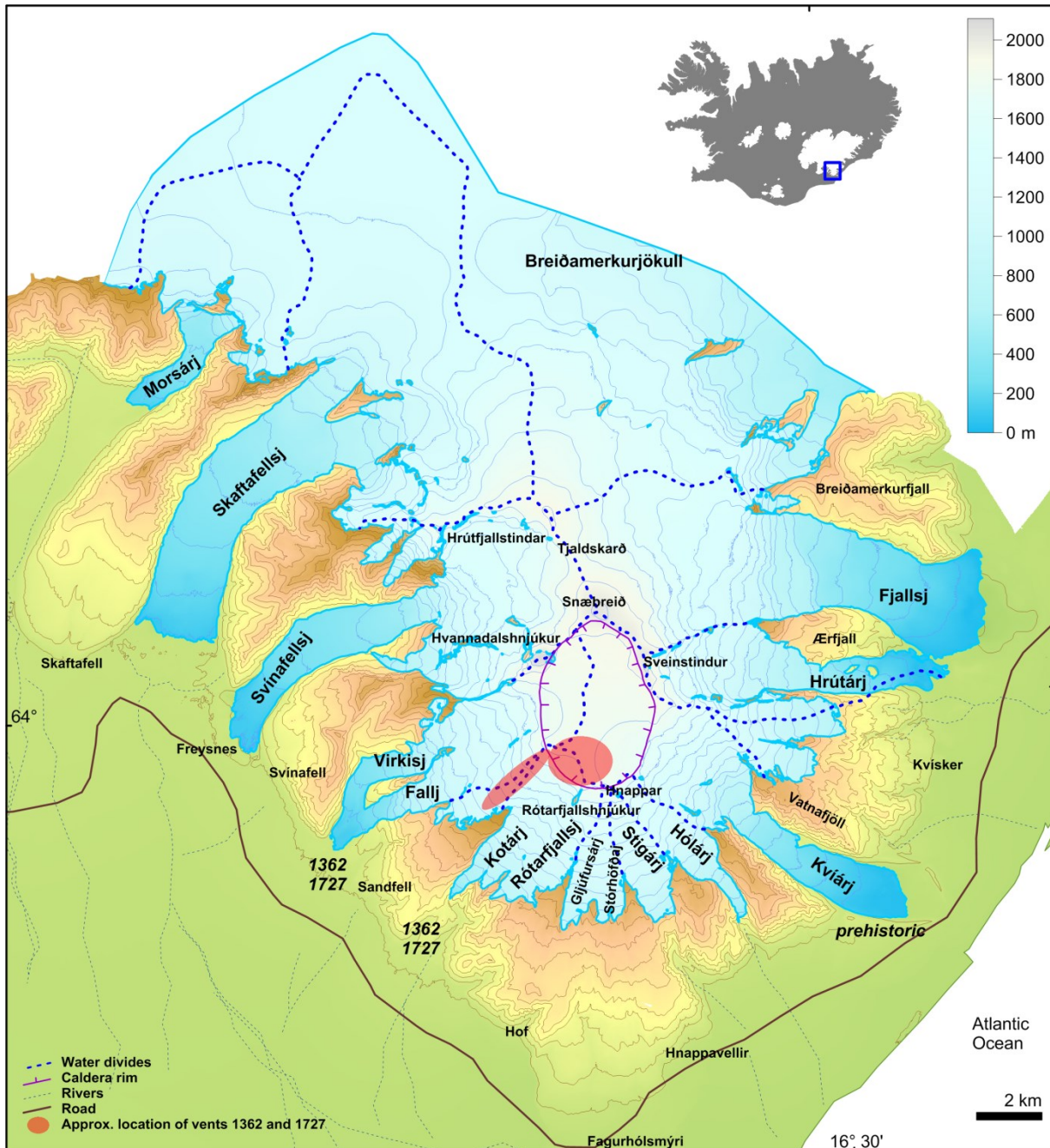


Figure III-1: Öreafajökull and surroundings, Surface topography and ice catchment basins. The main pathways of the jökulhlaups of 1362 and 1727 were down Falljökull and Kotárjökull.

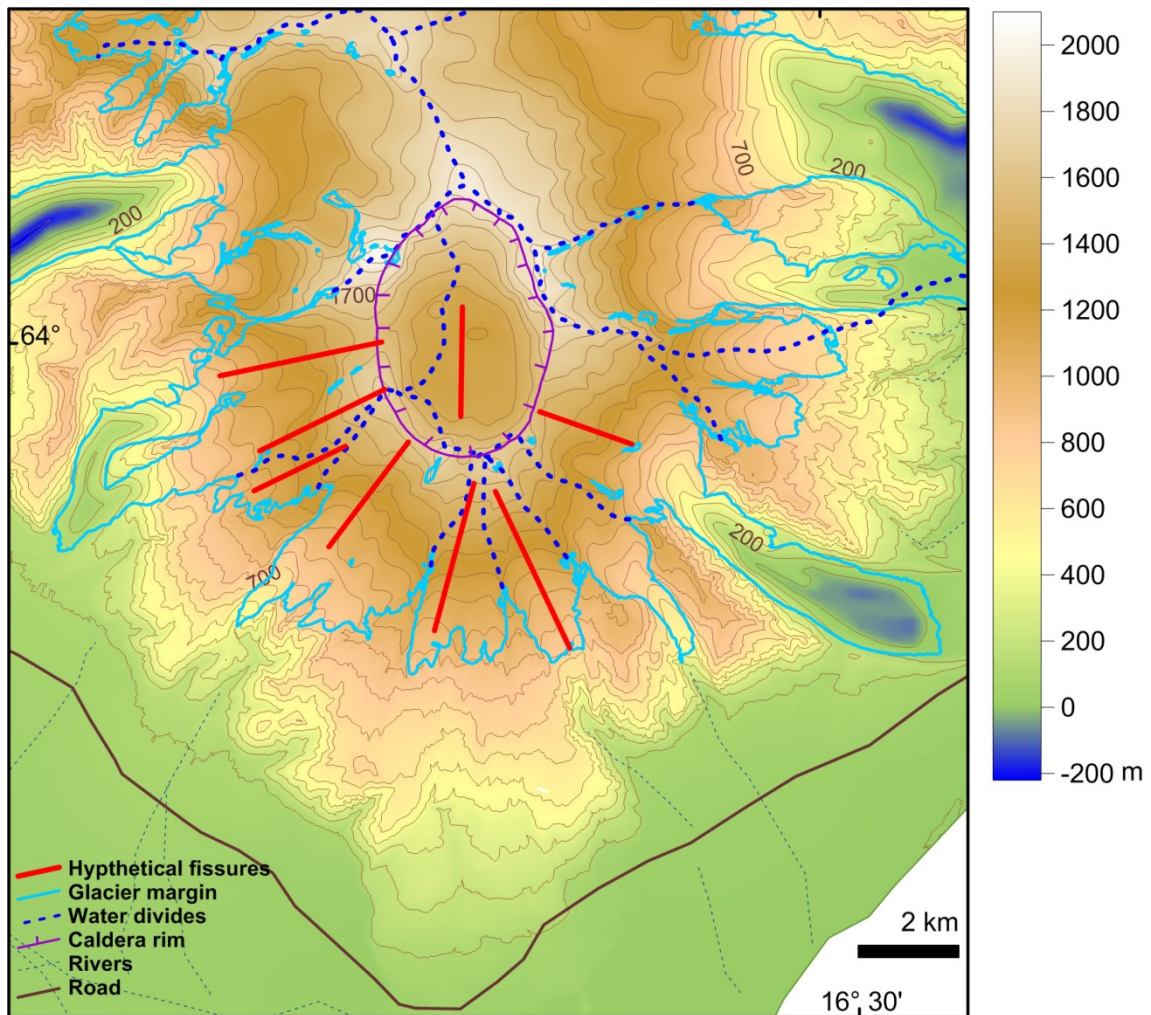


Figure III-2: Bedrock topography of Öraefajökull (after Magnússon et al. 2012b). The bottom of the caldera is an enclosed depression that would collect water if it were not ice-filled.

#### 4. Models of ice melting in eruptions

The conceptual models of magma melting considered here concur with the highest melting rates observed at certain ice thicknesses and eruption rates (Figure III-3):

- *Magma fragmentation under thick ice (>200 m)*, initially within a mostly water-filled cavity under a glacier, leading to highly efficient heat transfer from magma. An ice cauldron bounded by concentric crevasses may form on the surface as meltwater drains away subglacially. This type of event can be expected within the caldera of Öraefajökull.
- *Magma fragmentation within a fissure through ice*, with rapid initial widening of the fissure through melting. This model applies where rapid opening to the ice surface takes place and ice deformation is small in relation to vertical ice melting rates. This applies to relatively thin ice, but the thickness at which this occurs is expected to depend on the intensity of the eruption. In most cases this behaviour, as opposed to a subglacial water-filled cavity, is expected to occur in ice <200 m thick.
- *Snow and ice melting where pyroclastic density currents*, caused by plume collapse, flow over glaciers.

In Section 4.1 general considerations of heat content and calorimetric equations presented for heat transfer. In 4.2 the effect of an elongated vent (volcanic fissure) are considered, in 4.3 equations for thin ice

( $\sim < 200$  m) are presented and the thick ice in Section 4.4. In 4.5 estimates for the melting potential of pyroclastic density currents are given.

Table III-2: Maximum discharge ( $Q_m$ , in  $m^3/s$ ), mass eruption rate ( $\dot{M}$  in  $kg/s$ ), fissure length ( $l$ ) and mass eruption rate per unit length of fissure ( $\dot{m} = \dot{M}/l$ ) where known, for some Icelandic eruptions.

Eruption	Ref.	Magma type	$Q_m$ $m^3/s$	$\rho_m$ $kg/m^3$	$\dot{M}$ $kg/s$	$l$ $m$	$\dot{m}'$ $kg/m/s$
Hekla 1947	1	dacite	75,000	620	$4.7 \cdot 10^7$	4000	11600
Hekla 1991	2,3	andesite			$\sim 6 \cdot 10^6$	$\sim 4000$	$\sim 1500$
Gjálp 1996	4	Icelandite			$4 \cdot 10^6$	$\sim 4000$	$\sim 1000$
Grímsvötn 2004	5	basalt			$6 \cdot 10^5$	600	1000
Grímsvötn 2011	6	basalt			$1 \cdot 10^7$	1500	6700
Eyjafjallajökull 2010	7	trachyandesite			$1 \cdot 10^6$	1000	1000
Skaftáreldar* 1783	8	basalt	8,500	1450	$1.2 \cdot 10^7$	2200	5600
Askja 1875	9	rhyolite	125,000	-	$6.8 \cdot 10^7$	-	-

(1) Thorarinnsson (1967); (2) Gudmundsson *et al.* (1992); (3) Larsen *et al.* (1992); (4) Gudmundsson *et al.* (2004); (5) Jude-Eton *et al.* (2012); (6) Hreinsdóttir *et al.* (2014); (7) Gudmundsson *et al.* (2012); (8) Thordarson and Self (1993), Carey *et al.* (2010). \* For Laki (Skaftáreldar 1783) the values of  $Q_m$  and  $l$  given applies to the segment active at any given time (for details see Thordarson and Self (1993)).

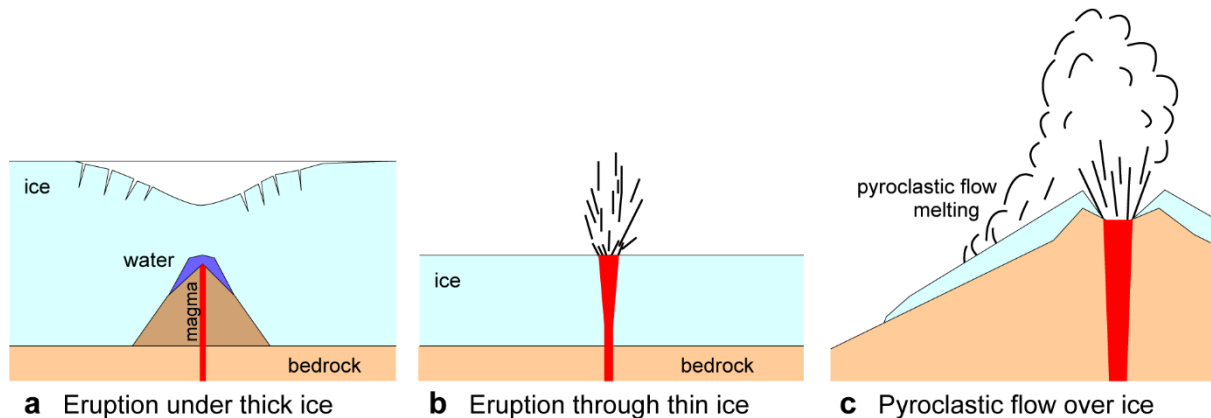


Figure III-3: The main scenarios for ice melting in eruptions at ice covered volcanoes. (a) Eruption under thick ice, (b) eruption through thin ice, and (c) pyroclastic density currents flowing over ice covered slopes (modified from Edwards *et al.*, 2015).

#### 4.1. Heat transfer and efficiency

In the end-member case when all the magma erupted is fragmented into glass particles, no crystallisation occurs (Carmichael *et al.*, 1974; Wohletz *et al.*, 2013). The products of

several recent subglacial eruptions suggest that this is a good approximation to the actual process (Gudmundsson, 2003; Jarosch *et al.*, 2008; Jude-Eton, 2012). Thus, it can be assumed that the latent heat of crystallization is insignificant. The processes that occur

when magma encounters ice are complicated, involving rapid cooling and breakup of the magma into mostly angular and blocky glass particles of dimensions <1 mm (Zimanowski, 1998; Zimanowski and Büttner, 2003). The cooling rates of these particles are characteristically in the range  $10^3$ – $10^5$  °C/s. As a result, rapid heating of water with a varying degree of boiling occurs (Figure III-4). This is expected to result in fast, partially forced convection that transfers magmatic heat to overlying ice with meltwater as the working fluid, probably with two phases present, liquid and steam (Gudmundsson, 2003; Woodcock *et al.*, 2012; Woodcock *et al.*, 2014). The details of these processes are beyond the scope of this report. Instead the heat transfer is approached through calorimetric considerations using extensively the concept of efficiency of heat transfer from the magma (Höskuldsson and Sparks, 1997; Gudmundsson, 2003).

The rate of heat transfer ( $dE/dt$ ) in a subglacial eruption from magma to the surroundings is given through:

$$\frac{dE}{dt} = f \rho_m Q_m C_g \Delta T = f \dot{M}_m C_g \Delta T \quad (1)$$

Here  $\rho_m$  is magma density,  $Q_m$  is the flow of magma ( $m^3/s$ ) with  $\rho_m Q_m$  being equivalent to the magma mass flux  $\dot{M}_m$  (in kg/s),  $C_g$  is the specific heat capacity of the glass (J/(kg K)),

$\Delta T = (T_i - T_f)$  is the change in temperature with  $T_i$  being magma temperature,  $T_f$  the temperature of the glass after cooling to ambient temperature, and  $f$  is efficiency of the heat transfer process (Gudmundsson, 2003) — see also Table III-1 for nomenclature. The simplifying assumption is made that  $C_g$  is a constant when in reality it is a moderately varying function of temperature. However, the error introduced by assuming constant specific heat capacity is small (Gudmundsson, 2003). Another factor not considered here is the energy required to fragment the magma (Schmid *et al.*, 2010). This may amount to 5–10% of the original thermal energy. However, this factor is only indirectly accounted for in the equations as an upper limit on the thermal efficiency.

The efficiency  $f$  is difficult to estimate directly. It was, however, done for the Gjálp 1996 eruption, defined as the ratio of the energy required to melt the ice during the eruption (30 September – 13 October 1996) and the total thermal energy of the erupted magma. Two definitions of thermal efficiency have been used: The efficiency of heat transfer from magma to ice, and the efficiency of heat transfer from magma to meltwater. These two definitions give different results when applied at the eruption site itself, where the meltwater usually has a temperature substantially above zero.

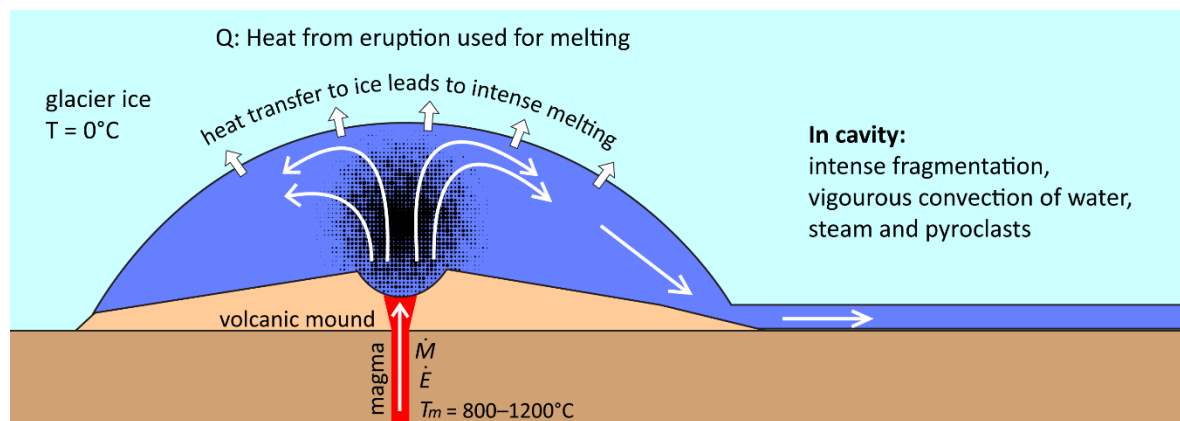


Figure III-4: Conceptual model of heat transfer and melting in an eruption under thick ice (>200 m).

If a jökulhlaup has a long subglacial path, this heat, initially stored in the meltwater, is released through ice melting along the flow path.

For Gjálp the efficiency of heat transfer to ice was 0.50–0.61 (50–61%) and to water 0.63–0.77 (63–77%) (Gudmundsson *et al.*, 2004). In most cases relating to jökulhlaup hazard, the efficiency of heat transfer to water is relevant because the melting along the path contributes to the meltwater generation. During some eruptions the efficiency of heat transfer to water may have been even higher than for the Gjálp event. This may have been the case during the Katla eruption of 1918, where the majority of the initially erupted material was volcanic glass transported with the meltwater (Tómasson, 1996; Larsen, 2000) — hereafter referred to as water-transported tephra. The temperature of these pyroclasts as they emerged with the floodwaters in 1918 was probably close to zero, way below the 200–300°C obtained as residual heat in the volcanic edifice built during the Gjálp eruption; a value obtained by considering heat released during post-eruption melting (Jarosch *et al.*, 2008).

Under a glacier, the heat transferred rate from magma is largely dissipated through ice melting. If it is assumed that the ice is temperate (at pressure melting point for ice – close to 0°C) as applies to Icelandic glaciers (e.g. Björnsson and Pálsson, 2008),  $\rho_i$  and  $\rho_w$  are the densities of ice and water respectively and  $L_i$  latent heat of solidification of ice, the melting rate  $Q_w$  (in water equivalent m<sup>3</sup>/s) is:

$$Q_w = \frac{\rho_i}{\rho_w} \frac{1}{\rho_i L_i} \frac{dE}{dt} = \frac{f \dot{M}_m C_g \Delta T}{\rho_w L_i} \quad (2)$$

This equation can be applied to all cases where an estimate of efficiency and mass flux can be made. The magnitude of some of the parameters is dependent on magma type, where  $\Delta T$  ranges from up to 1200°C for primitive basalts to ~800°C for rhyolites. Likewise,  $C_g$  is higher for basalts (1000–1200 J/kg K) than for rhyolites (~900 J/kg K) (e.g.

Höskuldsson and Sparks, 1997; Bacon, 1977).

## 4.2. Fissure eruptions

For a fissure eruption with length  $l$  and magma flux  $\dot{m} = \dot{M}/l$  per unit length of fissure (in kg/s m) equation (2) becomes:

$$Q_w = \frac{f l \dot{m} C_g \Delta T}{\rho_w L_i} \quad (3)$$

This equation could be used to calculate the mass flux in an eruption if both fissure length  $l$  and meltwater discharge  $Q_w$  are known. However, in practice this is difficult since independent estimates of the meltwater flow rate are often hard to obtain in real cases. The equation is nevertheless useful since it provides a way to estimate possible ranges of melting rates and hence jökulhlaup sizes in eruptions on ice covered volcanoes (Gudmundsson and Högnadóttir, 2005, 2006). Although the magma flow rates have only been estimated for a handful of subglacial eruptions, a considerable body of data exists on magma flow rates in e.g. effusive eruptions in Iceland and elsewhere (Table III-2).

## 4.3. Thin ice (less than ~200 m)

Experience from eruptions in Iceland and elsewhere suggests for basaltic and intermediate compositions, that all eruptions except the smallest ones starting under ice thicknesses <200 m melt their way through the overlying ice by forming cauldrons with vertical ice walls (Smellie, 2002; Gudmundsson, 2005; Magnússon *et al.*, 2012a). Observations are lacking for dacitic and rhyolitic eruptions within glaciers but it is expected that they would behave in a similar way. Within the walls, ice is completely melted away, but ice deformation and flow into the depression is relatively minor, except on steep ground where gravity pulls ice downwards into the crater from the uphill side. Thus a cauldron with very steep to vertical ice walls is typically formed around the eruption site.

In the case of a fissure eruption, the cauldron is elongated, forming an ice canyon reaching from the base of the glacier to the surface. Observations of the rate at which cauldrons widen can provide constraints on the melting rate. Table 3 shows the available data on the widening of ice cauldrons, based on observations of eruptions at Grímsvötn, Eyjafjallajökull and Deception Island.

#### 4.3.1. Widening of ice cauldrons

The widening rate of an ice cauldron (Figure III-5) can be used to estimate the approximate

melting rate in an eruption within a glacier characterized by thin ice (~200 m or less). If  $\rho_i$  and  $\rho_w$  are defined as before,  $h$  is ice thickness and  $l$  is the length of the eruptive fissure, an elongated ice cauldron is formed that acquires a width  $\Delta b$  during time  $\Delta t$ . The rate of melting is then given with:

$$Q_1 = \frac{\rho_i}{\rho_w} hl \frac{\Delta b}{\Delta t} \quad (4)$$

The most critical parameter here is  $\Delta b$ .

Table III-3: Dimensions and widening rates of ice cauldrons/canyons formed around volcanic fissures in eruptions under shallow ice. Estimates of parameters for equation (4) and (5).

Eruption	Width of cauldron: $\Delta b$ (m)	Time since start or eruption: $\Delta t$ (s)	$\frac{\Delta b}{\Delta t}$ (m/s)
Grímsvötn 1998	~100	~7200	$1.4 \cdot 10^{-2}$
Deception Island 1969	~100	~7200	$1.4 \cdot 10^{-2}$
Grímsvötn 2004	~400	~45000	$0.9 \cdot 10^{-2}$
Eyjafjallajökull 2010	~250	~25000	$1.0 \cdot 10^{-2}$

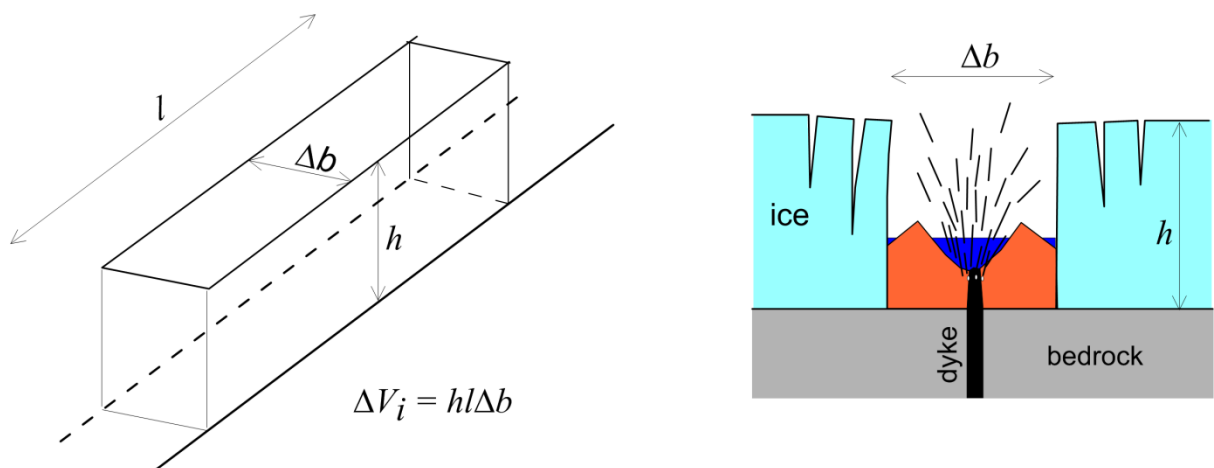


Figure III-5: Schematic setting for a volume model for melting rates in a fissure eruption on a flank where ice is thin (<200 m). From Gudmundsson and Högnadóttir (2005).

### 4.3.2. Melting rate per unit length of fissure

An alternative approach is to use a purely empirical equation, where the average melting rate per unit length of the volcanic fissure is obtained as the mean of the available data. The total melting rate is then a simple scaling with respect to the fissure length. The difference between this approach and equation (4) is that thickness of ice is not used as a variable. The melting rate factor  $q$  is obtained for each test case from:

$$q = \frac{\rho_i \Delta V_i}{\rho_w l \Delta t} \quad (5)$$

Here  $\Delta V_i$  is the volume of ice melted over time  $\Delta t$  and length of volcanic fissure is  $l$  as in eq. (4). The range of values obtained for the eruptions used in Table III-3 is 0.9–1.4 m<sup>2</sup>/s. The highest values are considered to be the most representative for the initial 1–2 hours and they are therefore used in our calculations.

The total melting rate in a fissure eruption using this approach is given by:

$$Q_2 = ql \quad (6)$$

Equations (4) and (6) are applied to estimate the melting rate in hypothetical fissure eruptions on the flanks of Öräfajökull. It should be noted that the equations provide estimates that only apply to the first few hours of an eruption starting under thin (<200 m) ice. After the initial phase, when the cauldron/canyon has reached a width of 200–300 m, the increased distance between volcanic fissure and the ice wall will lead to reduced melting as an increased fraction of the heat associated with the eruption is transferred to the atmosphere with the eruption plume.

### 4.4. Thick ice (>200 m)

When the ice thickness exceeds 200 meters, in all but the most powerful eruptions, the effects of ice flow are expected to begin to play a role, with meltwater draining away

from the eruption site in most cases, leading to the formation of an initial ice depression (ice cauldron) over the subglacial vents (Figures III-3a and III-4). The time it takes to melt through the ice and establish a connection to the atmosphere will be significant, and an interval will exist where the eruption is fully subglacial and meltwater drains away at a rate comparable to the rate at which meltwater is generated. During this subglacial period the melting rate will be governed by the magma flow rate (eq. 2).

Effusive, fully subglacial eruptions may occur at Öräfajökull. Equation (2) still holds but the efficiency is expected to be much less than the 0.6–0.8 used for fragmentation; values in the range 0.10–0.45, with the lower values applying to eruptions with high magma discharge (Gudmundsson, 2003).

Mass eruption rates (MER), observed during large eruptions in Iceland are in the range 10<sup>7</sup>–10<sup>8</sup> kg/s (Table III-2). The efficiencies used for magma fragmentation (0.6–0.8) translate to meltwater generation rates of 30,000–300,000 m<sup>3</sup>/s. These values are of the right order of magnitude compared to large historically documented jökulhlaups from Katla and Öräfajökull.

### 4.5. Pyroclastic density currents

Melting of snow and ice by PDC's is well documented for the eruptions of Redoubt in 1989–90 and 2009. Column collapses in vulcanian explosions lead to the flow of hot pyroclasts down the steep slopes of Drift Glacier, entrainment of snow and rapid melting. Debris flows caused by dome collapses had a similar effect. These melting events lead to lahars (hyperconcentrated floods) down the Drift River Valley. The peak discharges high in the valley have been estimated as 10<sup>4</sup>–10<sup>5</sup> m<sup>3</sup>/s (Waythomas *et al.*, 2013). The events were, however, of short duration and the peak discharges observed at the mouth of the valley were much reduced. Similar events were observed at Mount St. Helens in 1980–83 (Waite *et al.*, 1983).

At Nevado del Ruiz on 13 November 1985 a series of PDCs were formed over a period of a few minutes at the start of the main eruptive pulse of a VEI 3 eruption (Pierson *et al.*, 1990). These PDC's were initiated at the summit vent at an elevation over 5000 m. They swept across the 10 km<sup>2</sup> summit ice cap and within minutes of their start, dilute flows of water and tephra cascaded down the steep slopes into narrow canyons radiating outwards from the volcano. Within the canyons, the lahars accumulated more solid material, including loose sediments at the bottom of the canyons and tephra from the ongoing eruption. These lahars flowed along these canyons for tens of kilometres. One of them inundated the town of Armero, located at the mouth of a canyon, 74 km from the summit, killing 23 thousand people over the course of several minutes. From the perspective of lahar initiation, an important lesson from Nevado el Ruiz is that the ice and snow melting occurred over a period of only a few minutes.

The events observed in the eruptions mentioned above were of short duration and high discharge, but usually at short runout distances (<50 km). The pyroclastic density currents/debris flows causing them were moderate in size compared to what is to be expected in a major Plinian eruption such as occurred in Öraefajökull in 1362.

Walder (1999) studied melting of pyroclastic deposits on Mount St. Helens and came to the conclusion that pumice deposits melted a layer that was about the same thickness as the pyroclastic deposit. However, no models, comparable to those already presented for subglacial eruptions, have been published to estimate the melting rates and melted volumes generated by hot PDCs flowing over snow and ice. Observations and experimental results indicate that PDCs scour the underlying snow and ice surface, not only mechanically but also thermally (Walder, 2000a, b). The mechanical scouring occurs as the PDC erodes and excavates the underlying snow and ice. The thermal scouring follows

from heating of the ice and snow resulting in thermal convection that can promote fluidization of the pyroclast-snow-meltwater mixture (Walder, 2000a, b).

PDCs are characteristically dense, hot, ground hugging granular avalanches (Branney and Kokelaar, 2002; Roche *et al.*, 2013). The dilute end-member of a PDC, is the pyroclastic surge which is principally made of hot gas with pyroclastic particles suspended in the flow (e.g. Roche *et al.* 2013). For the case of ice surface melting, it is the dense types of PDCs that are relevant. It is not the intention here to go deeply into the physics of PDCs. Instead the following treatment will consider the thermal energy of PDCs and to what extent they can melt snow and ice.

In what follows, an attempt is made to quantify melting rates resulting from pyroclastic density currents flowing over snow and ice (Figure III-6). The key parameters are the mass eruption rate (MER), the mass of pyroclastic material in a collapsing plume event, the duration of collapse and the emplacement temperature  $T_e$  of the currents (the temperature of current when it first makes contact with snow/ice). We consider the case where, during an explosive eruption with a MER  $\dot{M}$ , the column collapses. The collapse occurs over time  $\tau$ . The total mass of pyroclastic material that collapses is:

$$M_p = \dot{M}\tau \quad (7)$$

A fraction  $\chi$  of this material entrains sufficient air to become buoyant and forms a secondary eruption cloud (phoenix cloud). This material does not contribute energy towards snow melting. The mass of pyroclastic material in contact with ice and snow is:

$$M_g = (1 - \chi)M_p = (1 - \chi)\dot{M}\tau \quad (8)$$

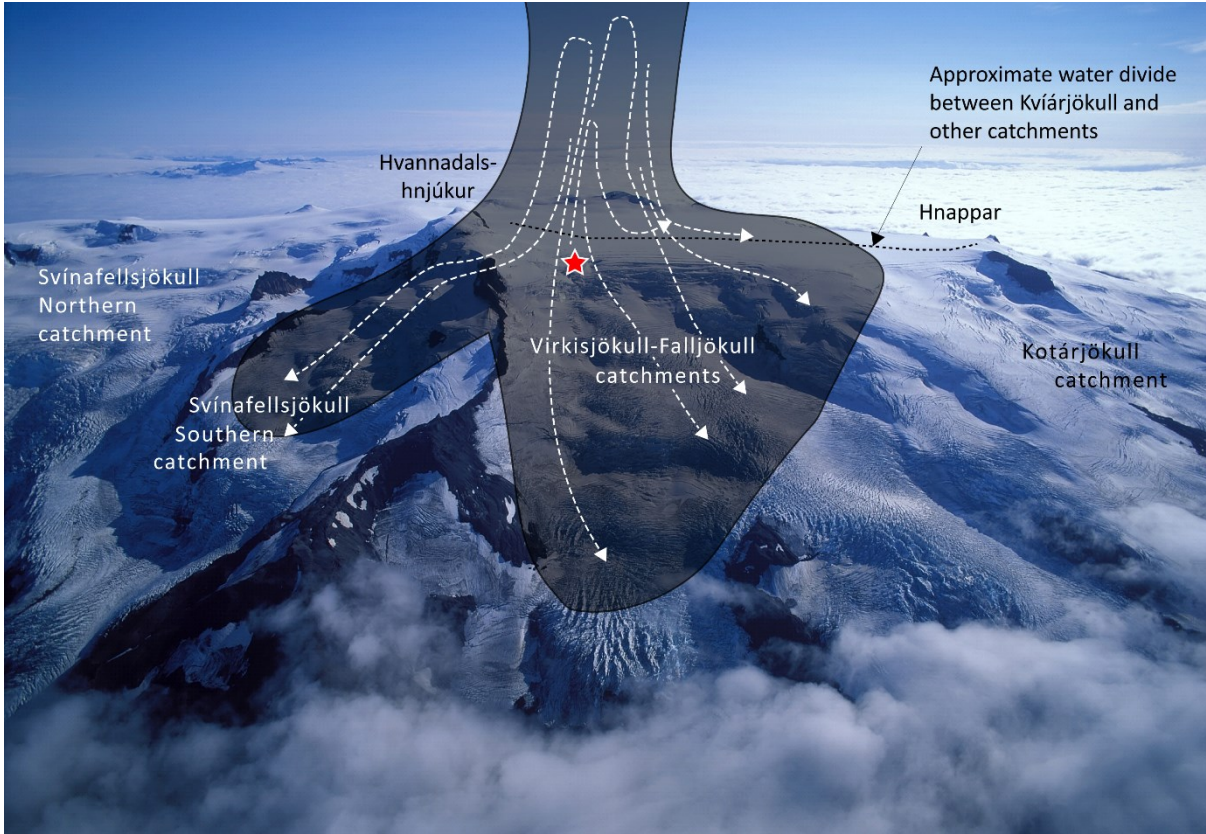


Figure III-6: Hypothetical setting for pyroclastic density current (PDC) generation in a Plinian eruption in the northwest part of the Öraefajökull caldera. The dark areas indicate the plume and the PDC. It is expected that a large PDC will cover a much greater area, reaching the lowlands beyond the volcanic edifice. Photo: Snævar Guðmundsson.

The energy that is available to melt snow and ice is therefore:

$$E_p = f(1 - \chi)\dot{M}\tau C_p(T_e - T_0) \quad (9)$$

Where  $f$  is the efficiency of the process,  $C_p$  is the specific heat capacity of the pyroclasts,  $T_e$  is emplacement temperature and  $T_0$  ambient temperature ( $\sim 0^\circ\text{C}$ ). It is to be expected that effective mixing of pyroclasts and snow will occur as the density current advances at high velocity along the surface, as it did at Nevado de Ruiz, Redoubt and Mount St Helens. The total amount of snow and ice melted from the surface of the glacier is:

$$V_w = \frac{E_p}{L_i\rho_w} = \frac{f(1-\chi)\dot{M}\tau C_p(T_e-T_0)}{L_i\rho_w} \quad (10)$$

The average melting rate (meltwater generation rate) for a given catchment is then found from:

$$Q_w = \xi \frac{V_w}{t_{run}} = \frac{\xi f(1-\chi)\dot{M}\tau C_p(T_e-T_0)}{L_i\rho_w t_{run}} \quad (11)$$

Where  $\xi$  is the fraction of the total pyroclastic density current generated that affects the catchment. For example, a large column collapse in a hypothetical major eruption with a vent in the western part of the caldera may lead to pyroclastic density currents that will partly overspill to the Svínafellsjökull catchment, partly flow down Virkisjökull-Falljökull and partly flow across the more southerly catchment of Kotárjökull and possibly further to the south.

Jökulhlaups could occur from all these catchments simultaneously as a result. The time  $t_{run}$  is the time it takes for a PDC to flow over the glacier and release its heat to the underlying snow and ice. The variable  $t_{run}$  is not well constrained, but it is here set as 10 minutes.

*Mass eruption rate (MER):* During major Plinian eruptions, usually erupting dacite or rhyolite (Table III-2), MERs of  $10^8$  kg/s occur in Iceland. The recent example is considered to be Askja 1875, since although the mean eruption rate did not quite reach this value (Table III-2), Carey *et al.* (2010) suggest that during the peak of the eruption the mass eruption rate was  $\sim 10^8$  kg/s. Other eruptions of this magnitude include Öræfajökull 1362, Hekla 1104, Hekla 3, Hekla 4 and Katla  $\sim 10$ –11 kyr BP (Vedde ash eruption). We therefore use  $10^8$  kg/s for estimating the possible effects at a major eruption in Öræfajökull.

*Heat transfer efficiency:* The efficiency of melting by PDCs is highly uncertain and depends on the thermal effects of pyroclast interaction with snow and ice, the degree of scouring and entrainment of the snow and ice and the interplay among these processes. As in the other cases considered, it is the fast or semi-instantaneous rate of heat loss that is relevant. In the light of the observed melting at e.g. Redoubt and Nevado de Ruiz, it is likely that the efficiency can be comparable to that of a subglacial eruption with fragmentation, requiring very effective mixing of the pyroclasts with ice and snow. The converse is also possible, that very little melting occurs if the glacier surface is smooth, without crevasses and covered by a tephra layer that would act as an insulation. Considering that plausible worst case scenarios are being studied, a rather high value of  $f = 0.5$  (50%) is adopted.

*Partitioning between PDC and phoenix cloud:* The partition between the ground-hugging component of the PDC and a phoenix cloud can only be approximated crudely; we will use a value of 0.5 here.

*Emplacement temperature:* Finally, for pyroclastic density currents not associated with fragmentation by external water, emplacement temperatures have been estimated as ranging from  $\sim 300^\circ\text{C}$  to at  $550^\circ\text{C}$  (e.g. Mandeville *et al.*, 1994; Scott and Glasspool, 2004). As seen from the above discussion, the estimates obtained are very crude, but are expected to give the approximate order of magnitude. For wet (phreatomagmatic) eruptions base surges are common but the temperature of these is low ( $< 100^\circ\text{C}$ ). In recent eruptions in Iceland (Grímsvötn, Eyjafjallajökull) base surges have been frequently observed but have not resulted in significant ice melting. Thus, we only consider the case where the vent has melted a large enough opening in the glacier that external water flows away from the vent and is not a factor in influencing eruption dynamics. This exclusion of external water allows hot pyroclastic flows to occur, provided eruption rates are high enough. In our estimates for Öræfajökull, we therefore use  $T_e = 550^\circ\text{C}$ .

In Figure III-7, the melting rate resulting from a pyroclastic density current obtained for the parameters specified above is shown as a function of  $\xi$ . Considering the magnitude of the event analysed (MER  $10^8$  kg/s), it would be unlikely that all the melting would occur in a single catchment ( $\xi = 1.0$ ); a more likely scenario would be  $0.2 < \xi < 0.5$  with melting spread over two or more catchments.

## 5. Jökulhlaups resulting from subglacial eruptions

The analysis presented in Section 4 gives plausible maximum melting rates for various eruptive scenarios. In this section, the transport of meltwater from the eruption site to the edge of glacier and the effects of entrainment of pyroclasts as water-transported tephra and ice is considered, in particular the effect of these processes on maximum discharge and transport properties of the jökulhlaups.

## 5.1. Subglacial hydrology

For a glacier that is a few hundred meters thick, any water at the base of the glacier is pressurised. This implies that the water pressure is similar to the lithostatic pressure exerted by the load of the overlying ice (e.g. Björnsson, 1988, 2003). Thus, flow paths of water at the base are controlled by a static fluid potential:

$$\varphi = (\rho_w - \rho_i)gz_b + \rho_i gz_s \quad (12)$$

Where  $g$  is acceleration due to gravity and  $z_b$  and  $z_s$  are the height of respectively the glacier base and the ice surface (Björnsson, 1976).

Flow paths of meltwater at the glacier base will be down the gradient of this potential. The potential (eq. 12) highlights the importance of the slope of the ice surface as it is 10 times more influential in driving water flow than is the bedrock slope. This implies that water can flow uphill provided the slope of the ice surface is opposite to that of the bedrock and the bedrock slope is less than 10 times greater than the surface slope. This is highly relevant to Öraefajökull, where the caldera bottom is an enclosed bedrock depression (Magnússon *et al.*, 2012b).

In a glacier the slope of the ice surface is generally away from the centre towards the edge of a glacier. This drives water from the interior towards the glacier margins. Moreover, conditions for water accumulation are seldom met, except in places where sustained geothermal activity has created deep depressions in the glacier surface. This is the case at Grímsvötn and Skaftárkatlar (e.g. Björnsson, 2003) and in isolated smaller cauldrons in such as Mýrdalsjökull (Gudmundsson *et al.*, 2007).

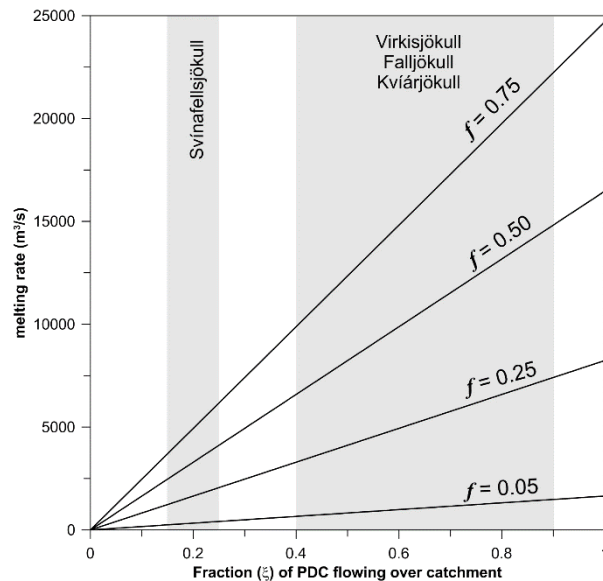


Figure III-7: Estimates of the rate of melting within an ice catchment area due to flow of a pyroclastic density current over snow and ice derived using equation (11). The mass eruption rate is assumed to be  $\dot{M} = 10^8$  kg/s and the duration of collapse  $\tau = 120$  s. Values for different values of efficiency of heat transfer ( $f$ ) are shown, with  $c = 0.5$ ,  $T_e = 550^\circ\text{C}$ ,  $T_0 = 0^\circ\text{C}$  and  $C_p = 1000$  J/(kg °C). Likely maximum values of  $\xi$  for the main catchments are indicated.

In regions where ice thickness is substantial (>200 m) the static fluid potential is expected to dictate flow paths of meltwater.

For most regions within glaciers in Iceland and elsewhere, conditions are such that water will have a tendency to flow away from the eruption site. As a consequence, a depression will form in the ice surface above the subglacial eruption site. The resulting slope in the ice surface into the depression will cause ice flow into it, partly counteracting the subsidence. It is during this, initially fully subglacial stage, that ice melting in a subglacial eruption is expected to be highest.

## 5.2. Transport of solids with meltwater, bulking of jökulhlaups and lahars

Jökulhlaups caused by volcanic eruptions under glaciers are usually a mixture of water, sediments and ice. The sediments are usually pyroclasts from the eruption. Jökulhlaups can be water floods (often defined as having <40% of the mass as solids) or lahars, that is hyperconcentrated (40–80% solid) or debris flows (>80% solid material) (Beverage and Culbertson, 1964).

In jökulhlaups, the solid concentration is expected to depend on several factors and there is no straightforward way to constrain the expected ratio of liquid and solid in the flow. The type of eruption (effusive on one hand and fragmentation on the other) is of major importance since fragmentation leads to a high supply of fine-grained pyroclastic material that can easily be transported with meltwater. The steepness of the flow path of the meltwater down the slopes of a volcano is another factor that should lead to increased sedimentation. Detailed analysis of possible scenarios is beyond the scope of this chapter but it is important to consider the possible effect of the solid fraction originating as pyroclastic material at the source. This material can in some cases mostly be transported with the meltwater with minor amounts being left at the eruption site. In other cases most of it may be stored at or near the vents forming a volcanic edifice. In the former case the solids make up a substantial part of the flow, resulting primarily in hyperconcentrated flows.

The meltwater generated by subglacial eruptive activity is defined by eq. (2). The ratios of the mass generation rate of meltwater  $\dot{M}_w$  and pyroclasts  $\dot{M}_p$  (assumed to equal the MER  $\dot{M}_m$  during full fragmentation) can be derived from equation (2) resulting in equation (13):

$$\frac{\dot{M}_p}{\dot{M}_w + \dot{M}_p} = \frac{1}{1 + \frac{f C g \Delta T}{L_i}} \quad (13)$$

Here  $\Delta T$  is the difference in temperature of the water as it is released from the glacier and the temperature of the magma. Other parameters are defined as before. The volume ratios can also be determined using the densities of water ( $\rho_w$ ) and pyroclasts ( $\rho_p$ ) with  $Q_p$  being the volume flux of pyroclasts and  $Q_w$  the flux (volumetric flow rate) obtained from equations (2), (4) or (6):

$$\frac{Q_p}{Q_w + Q_p} = \frac{1}{1 + \frac{\rho_p f C g \Delta T}{\rho_w L_i}} \quad (14)$$

Equations (13) and (14) can be used to evaluate the potential concentration of water-transported tephra in jökulhlaups. In Figure III-8 the variations in solid mass and volume fractions (eq. 13 and 14) are shown as a function of efficiency. If all the solid material is transported with the meltwater, the resulting jökulhlaup will have properties as shown by the solid curve.

If a fraction of the erupted material stays at the eruption site the concentrations of solids will be lower, within the shaded region.

The difference between a subglacial eruption and the melting by a PDC lies in the different temperature differences, 1100°C for the eruption and 550°C for the pyroclastic flow, resulting in about 50% less melting per unit mass of a pyroclastic density current. This suggests that PDCs may be more likely to produce hyperconcentrated-flow lahars than are the subglacial eruptions, in agreement with the observations from Redoubt, Mount St. Helens and Nevado de Ruiz mentioned previously.

### 5.3. Discharge of jökulhlaups and lahars

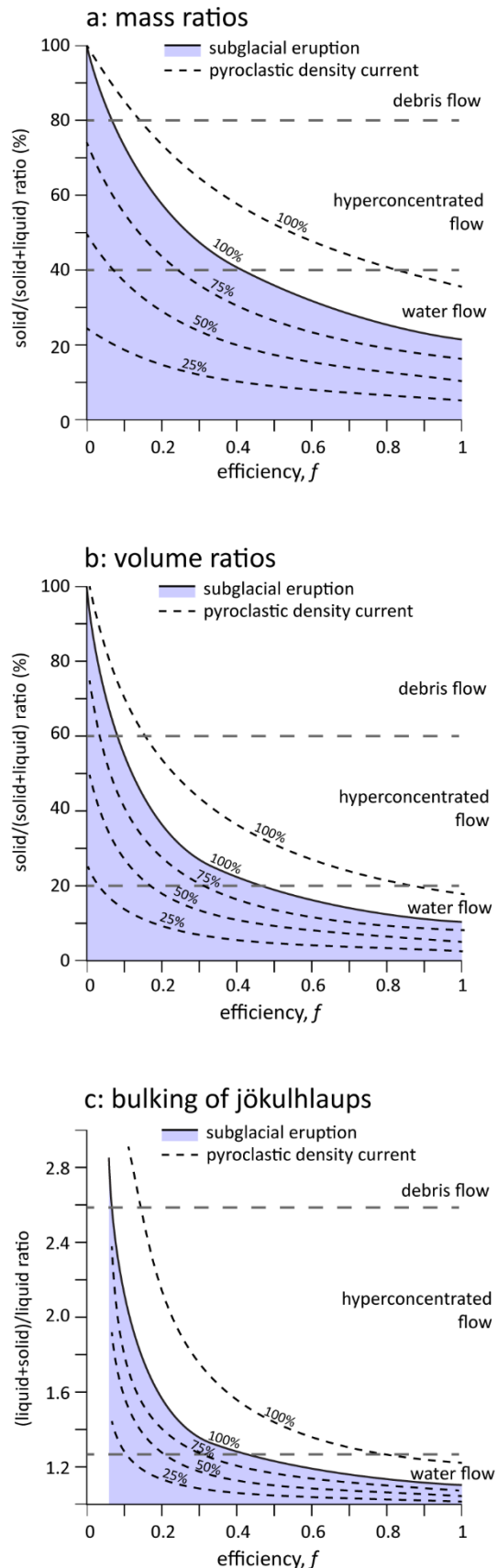
#### 5.3.1. Flow rates with bulking, flank eruptions

From the discussion in 5.2 it is clear that in steep terrain the volume of water-transported tephra should be taken into account when evaluating the potential discharge of jökulhlaups. If  $Q_w$  is either  $Q_1$  as obtained from eq. (4) or  $Q_2$  from eq. (6), the effect of bulking is accounted for by combining these equations with (14) as:

$$Q_T = \left(1 + \frac{\rho_w}{\rho_p} \frac{L_i}{f C_g \Delta T}\right) Q_w \quad (15)$$

This equation is used to calculate the maximum discharge for fissure eruptions on the ice-covered slopes of Öräfajökull. It is assumed that that the efficiency is 0.35–0.40, implying a solid mass fraction in the range 40–45%, reaching hyperconcentrated values and the generation of a lahar with  $Q_T = 1.25Q_w$ . During the 2010 Eyjafjallajökull eruption, jökulhlaups that formed during in the first two days of the eruption had a solid volume fraction of  $26 \pm 10\%$  (Magnússon *et al.*, 2012a), thus these estimates appear reasonable.

Figure III-8: Effects of pyroclast entrainment at the eruption site. a) Mass ratio of solids relative to the sum of solid and meltwater generated as a function of efficiency of heat transfer. The solid line shows 100% entrainment (all erupted material entrained in jökulhlaup). The broken lines show 75%, 50% and 25% entrainment. Possible bulking due to entrainment of material on slopes below eruption site is not considered. The dotted line shows mass ratios for 100% entrainment by pyroclastic density currents. b) Volume ratios of solid relative to the sum of solid and meltwater generated. c) Increase in volumetric flow rate due to entrainment of pyroclasts.



### 5.3.2. Discharge for eruptions under thick ice in caldera

For eruptions within the caldera, it is unclear how much water-transported tephra would be entrained by meltwater. The water would have to flow over a bedrock ledge for both outlets of Kvíarjökull and Virkisjökull-Falljökull. This means that the fluid potential gradient out of the caldera is smaller than on the slopes or would occur if no bedrock ledge was present. This could result in less sediment transport in a caldera eruption, but no model or theory exists on which to base an estimate. It will therefore not be attempted here to make such an estimate, apart from stating that 100% removal is highly unlikely because of the bedrock dam, with 50–75% removal being plausible worst cases. Using Figure III-8b, and efficiency of 0.6–0.8 for fragmentation as before, leads to a volume fraction of solids generated in the range 14–19%. Assuming 50–75% entrainment, this translates to 7–14% volume fraction in a jökulhlaup.

In the largest jökulhlaups with discharges of several tens of thousands of cubic meters per second, glacier termini can be extensively broken up by hydraulic fracturing and other mechanical disturbances. Tómasson (1996) estimated that the ice blocks amounted to 10–15% of the volume of the 1918 jökulhlaup of Katla. If a large jökulhlaup is generated through magma fragmentation under ice and the erupted material is mostly transported downslope with the meltwater as water-transported tephra, the combined bulking effect of the tephra entrainment (of 7–14%) and the ice blocks (10–15%) is 17–29%. The mean of this is 23%, not significantly different from the 25% bulking used for a flank eruption (see 5.3.1 above). We therefore apply the same multiplication factor of 1.25 to values calculated using eq. (2) or  $Q_T = 1.25Q_w$ . Thus, equation (16) is applied to both caldera and flank eruptions and accounts for the solid and liquid components of the flow where:

$$Q_T = 1.25Q_w \quad (16)$$

### 5.3.3. Discharge of lahars resulting from pyroclastic density currents

Equation (11) is used to estimate the mean flow rates of meltwater from a pyroclastic density current. The values of  $\xi$  (the proportion of current affecting a single catchment) is approximated by considering that collapse of a large eruption plume will direct pyroclastic debris over a relatively large sector of the flanks. The results of applying equation (11) are shown in Figure III-7. As indicated in 5.3.2, jökulhlaups resulting from pyroclastic density currents are expected to have higher proportion of solid material mixed with the meltwater, due to the lower emplacement temperature.

## 5.4. Propagation times of jökulhlaups and lahars

From the viewpoint of melting rates and delivery of meltwater to outlet glaciers on Öräfajökull eruptions, three different settings have been defined:

1. Eruptions within the Öräfajökull caldera.
2. Fissure eruptions on the flanks of the volcano, outside the caldera.
3. Melting during an explosive eruption by pyroclastic density currents flowing over the glacier surface.

For analysing these different settings, we define the following time intervals (Figure III-9):

- a) Eruption Onset Time (EOT): The time it takes for an eruption to start and establish a circular or elongated vent.
- b) Subglacial Transport Time (STT): The time it takes for meltwater to reach the surface of the glacier on the volcano flanks or its outlet glaciers. This concept is useful for eruptions on volcanoes with considerable ice surface and bedrock relief, e.g. Katla, Eyjafjallajökull and Öräfajökull where most or all of the meltwater flows on the surface down the steep slopes after flowing along a subglacial path near the source. For an eruption and jökulhlaup at volcanoes covered

by large glaciers, such as Grímsvötn, supraglacial flow rarely occurs except as overspill near the terminus. For these events the STT should be taken as the total time of transport from the source to the point of outflow at the surface.

c) Flank Transport Time (FTT): The time it takes the flood to traverse the flanks of the volcano, from the point it emerges from base of the ice or, where flow becomes established on the surface of the glacier (e.g. as a lahar after initial melting by a pyroclastic density current). This is the time estimated in Chapter IV (Helgadóttir *et al.*, 2015).

Data on subglacial eruptions and meltwater travel time are given in Table 4. Data on Katla prior to 1918 is limited since eruption rate cannot be estimated in any meaningful way, given that the information is on timing of earthquakes, sighting of eruption plumes and times of jökulhlaups.

For eruptions within the Öräfajökull caldera, onset time, subglacial transport time and flank transport time need to be added to obtain an estimate of the time between the start of an eruption and the arrival of a jökulhlaup in the lowlands beyond the volcano. The effects of these eruptions is expected to be similar to Katla eruptions. The ice thickness is comparable, 400–500 m as opposed to 400–700 m at Katla. However, the distance from the vent to the glacier terminus is smaller for Öräfajökull than it is for Katla, or 7–11 km as opposed to about 17–20 km for Kötlujökull.

#### 5.4.1. Eruption Onset Time (EOT)

For a large eruption ( $MER > 10^7$  kg/s) the timing of the initial arrival of magma at the surface (in this case the base of the glacier) and the formation of a fully established vent or fissure and the maximum MER, can be as low as 15–30 minutes. The 1947 Hekla eruption provides a similar example (Thora-

rinsson, 1954). Many basaltic eruptions also grow rapidly to a peak MER (e.g., the Krafla eruptions of 1975–1984; Einarsson, 1991). For most andesitic stratovolcanoes, a vent clearing phase on the order of 24 hours is common, often preceding the maximum MER during a vulcanian to Plinian phase (e.g. Bull and Buurman, 2013; Siebert *et al.*, 2015). For Öräfajökull hazard estimates, we adopt the lower value, of **15 minutes for EOT**. This time applies to both caldera and flank eruptions.

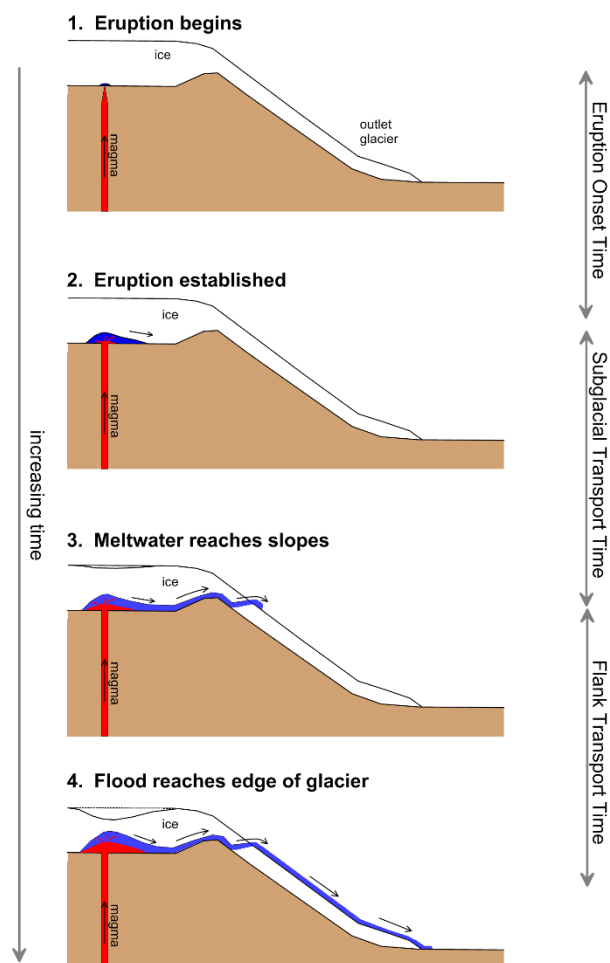


Figure III-9: Schematic setting for an eruption within Öräfajökull caldera and the eruption onset time (EOT), subglacial transport time (STT) and flank transport time (FTT).

Table III-4: Observed subglacial eruptions and travel times of meltwater.

	Initial ice thickness (m)	Initial Mass Eruption Rate (MER) ( $10^6$ kg/s)	Melting time (hours)	Heat transfer rate ( $\text{MW m}^{-2}$ )	Glacier path (km)	Av. glacier path gradient	Glacier travel time (hours)	Av. advance velocity (m/s)
Gjálp 1996	600	2-4	30	1.6	15	-	-	?
Gjálp 1996 jökulhlaup	-	-	-	-	50	0.0003	10	1.4
Eyjafjallajökull 2010	200	0.5-1	4	4.3	5	0.27	5.5	0.25
Katla 1918	400	50-100	1-2	30	17	0.07	1-2	2.4-4.8
Katla 1660	(500)	?	(1)	-	(17)	(0.07)	(2-4)	-
Katla 1721	(500)	?	(<4)	-	(17)	(0.07)	(<4)	-
Katla 1755	(500)	?	(<6)	-	(22)	(0.06)	(<3)	-
Katla 1823	(500)	?	(<2)	-	(17)	(0.07)	(<3)	-
Katla 1860	(500)	(1-10?)	(<10)	-	(17)	(0.07)	(<10)	-

Sources: Gudmundsson *et al.* (2004), Magnússon *et al.* (2012), data in Larsen *et al.* (2013)

#### 5.4.2. Subglacial Transport Time (STT)

The time it takes meltwater after the start of an eruption to propagate under ice from the eruption site until it reaches the slopes and may partly flow subaerially is highly uncertain. No theory backed up by empirical data exists as yet to calculate such times. Inferences can be made from empirical data in Icelandic eruptions, notably the Eyjafjallajökull eruption in 2010, Katla eruption in 1918 and indirect evidence from some earlier Katla eruptions. During the 2010 Eyjafjallajökull eruption, the STT was 3–4 hours (Magnússon *et al.*, 2012a), even though the transport length under ice was only 1.5–2 km. Beyond that distance, the flood was mostly supraglacial. For **flank eruptions** this time merges with the flank transit time and should be taken as equal to zero. For **caldera eruptions** in Öräfajökull the meltwater will travel 1–1.5 km (Virkisjökull) and 1–3 km (Kvíarjökull) before it can be expected to breach the surface and propagate subaerially from then on as observed at Eyjafjallajökull in 2010 (Magnússon *et al.*, 2012a). Using the minimum distance of 1 km for both cases to obtain the likely minimum subglacial transport time, and the advance velocities

from Table III-4 we obtain a maximum STT of 60–80 minutes (similar to Eyjafjallajökull 2010) — a plausible value for a small to moderate eruption within the caldera. Minimum STT is 3–7 minutes (right order of magnitude for Katla 1918). The fact that there is a high bedrock step that the meltwater from a caldera eruption in Öräfajökull has to overflow is not taken into account. In the absence of a tested model for the propagation of such a flood under the glacier, no reliable estimates can be obtained on the likely delay that this may cause. To be conservative, this possible delay is ignored here, and the minimum values are adopted. Thus we use a STT of 30 minutes for small to moderate eruptions in the caldera and a value of 5 minutes for large eruptions.

**Caldera eruptions:** The combined minimum onset and subglacial transport times are defined as 15 + 30 minutes = **45 minutes for a small to moderate eruption**. For a **large eruption** this combined time is 15 + 5 minutes = **20 minutes**.

**Flank eruptions:** Here only the onset time is relevant, taken as **15 minutes**.

### 5.4.3. Flank Transit Time (FTT)

The Flank Transit Time can be approximated for some past eruptions on the basis of observations and it can be estimated using flood routing. Here the Samos code, initially written to simulate flow of snow avalanches is used (Hákonardóttir *et al.*, 2005). The flank transit times, flow velocities, inundation zones and water depths are not the topic of this chapter. They are considered in detail in Chapter IV (Helgadóttir *et al.*, 2015) and therefore not estimated here.

### 5.4.4. Onset times and occurrence of pyroclastic density currents

Pyroclastic density currents should **not happen** at the very beginning of an eruption, since an ice cauldron or a wide fissure would have to be melted out before conditions for pyroclastic density currents are established. If we define the onset time of PDCs as the time from start of collapse until a flood is established on the upper slopes, this time is very short, **of order 5 minutes**.

PDCs and associated jökulhlaups can take place at any time after an eruption has established a vent open to the atmosphere, provided the eruption rate is high enough ( $>5 \times 10^7$  kg/s). This eruption rate need not be sustained, as discrete explosions can generate substantial PDCs.

### 5.4.5. Hydrographs of jökulhlaups

The hydrographs of jökulhlaups from all types of events considered can vary depending on conditions at the eruption site and the characteristics of the jökulhlaup path. Data on hydrograph shape for jökulhlaups caused directly by eruptions are limited, but rapid approximately linear increase in discharge is observed in many cases (e.g. the jökulhlaups from Eyjafjallajökull in 2010; Gudmundsson and Larsen, 2013). Observations of lahars from Redoubt in 2013 and Nevado del Ruiz 1985 also show the initial advance of a flow front, possibly followed by repeated waves of high discharge (Waythomas *et al.*, 2013; Pierson *et al.*, 1990). Hydraulic simulations of Katla jökulhlaups

(Hólm and Kjaran, 2005) were conducted using a simple triangular-shaped hydrograph with a linearly rising discharge, followed by a period of maximum discharge and a period of linear decline. This approach is applied in this study. For hazard purposes at Öraefajökull, where the effects of the jökulhlaups in the few-kilometres wide strip of lowland below the slopes are of primary interest, the most important parameters are the rate of increase of discharge and the peak discharge. The selected initial hydrographs are shown in Figure III-10.

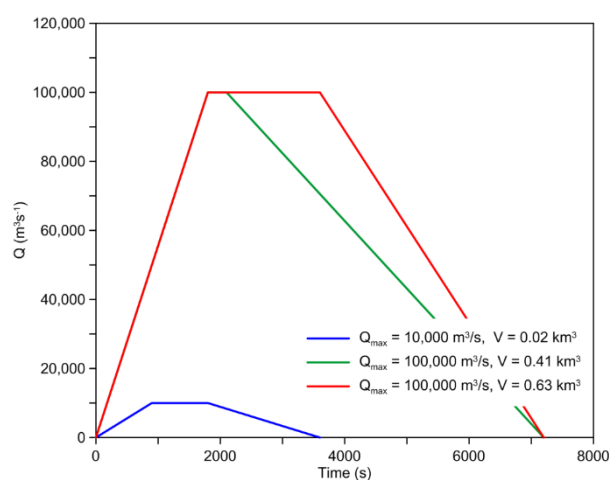


Figure III-10: Plausible hydrographs for jökulhlaups caused by eruptions at Öraefajökull. A discharge of  $10,000 \text{ m}^3/\text{s}$  applies to a moderate flank eruption, while the other two cases ( $Q_{\text{max}} = 100,000 \text{ m}^3/\text{s}$ ).

These hydrographs are applicable to situations where the meltwater emerges high on the flanks. The slope of the rising limb and time to peak discharge should reflect the fast but yet not instantaneous increase in melting during the eruption onset time.

It is possible that the time to peak discharge is considerably faster than estimated. However, the most likely scenario where this could happen is when meltwater is initially retained at the eruption site or the subglacial transport time is slow, possibly due to low potential gradient between the eruption site and the caldera rim.

## 6. Results

The melting potential and likely initial maximum discharges of jökulhlaups resulting from eruptions on Öraefajökull are presented in Tables III-5, III-6 and III-7, with the three main scenarios in each table: Flank eruptions, caldera eruptions, and pyroclastic density currents during an ongoing eruption.

### 6.1. Maximum discharge for fissure eruptions on ice covered flanks

The hypothetical fissures considered are shown in Figures III-11 and III-12. The results for  $Q_w$  calculated from both eq. (4) and (6) are given in Table III-5 and the higher of the two values is used to estimate  $Q_T$  for a plausible scenario using equation (16).

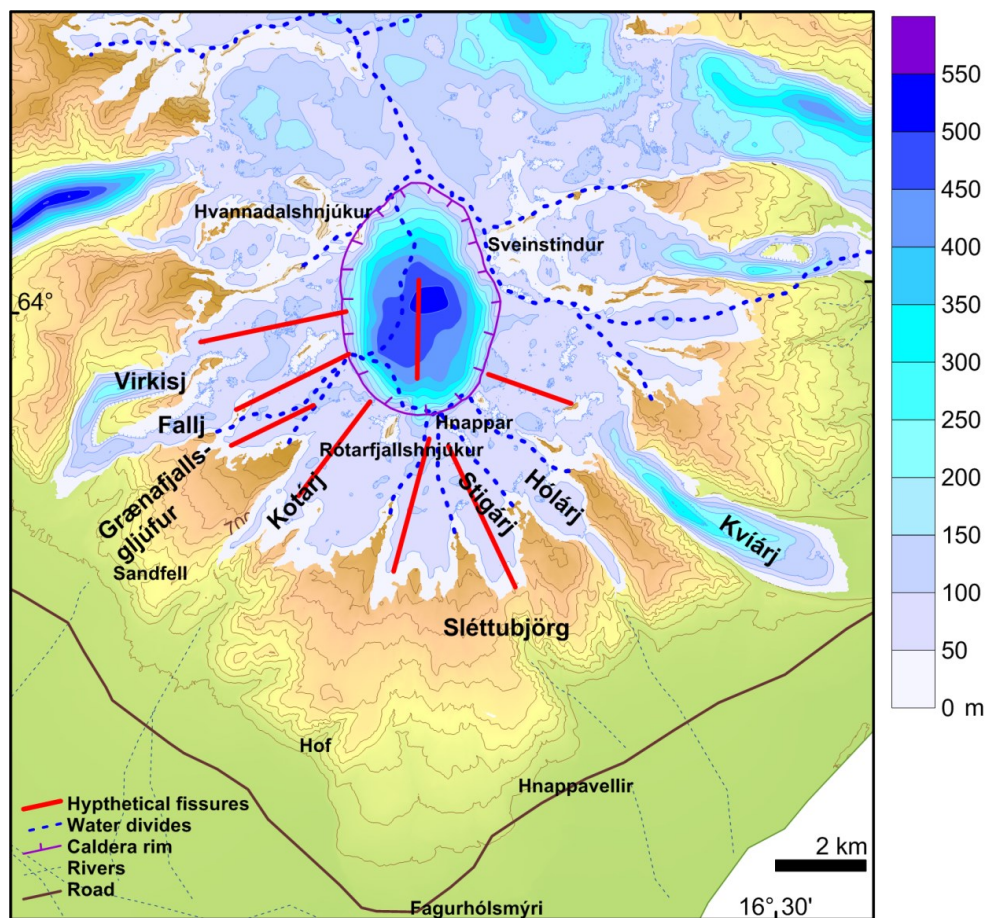


Figure III-11: Ice thickness map of Öraefajökull (after Magnússon et al., 2012b). Hypothetical volcanic fissures on the flanks and within the caldera of Öraefajökull, used to calculate possible discharge of jökulhlaups based on ice thickness and fissure length (Table III-5).

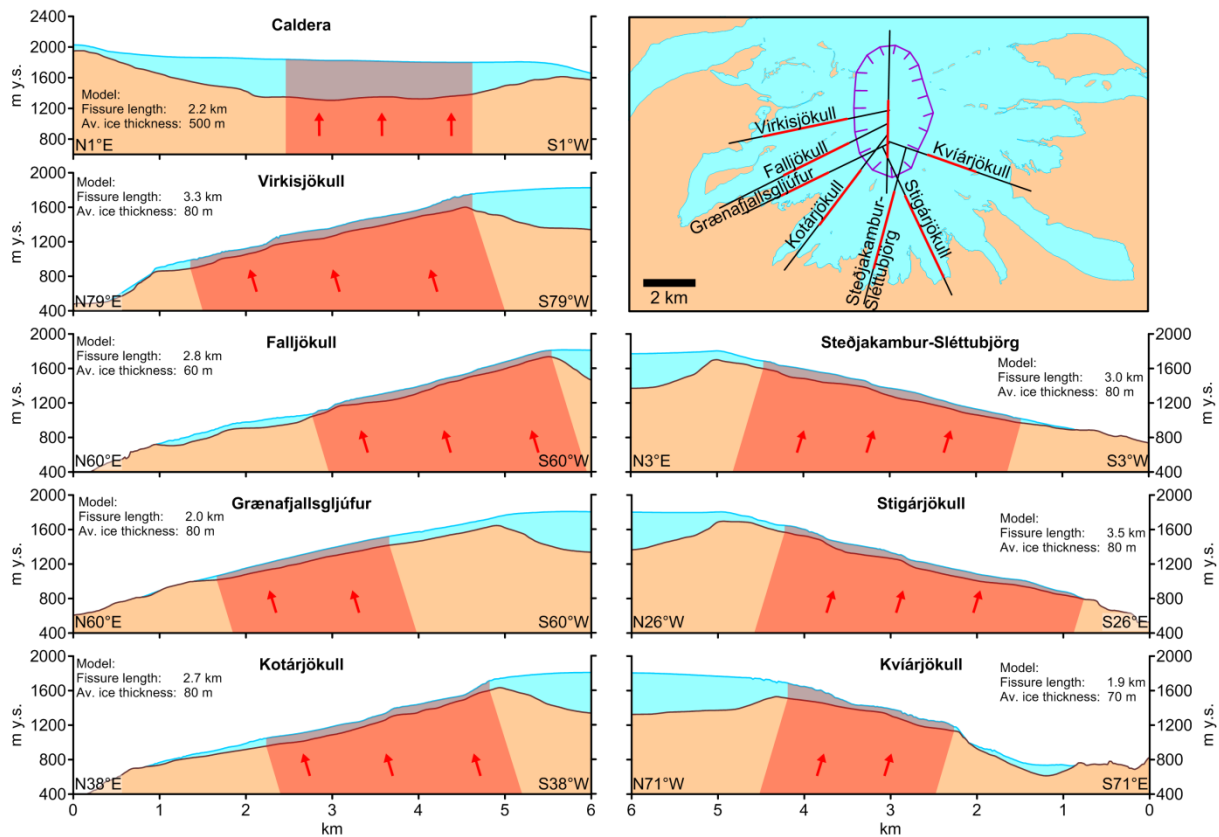


Figure III-12: Cross sections of bedrock and ice cover at locations of hypothetical fissure eruptions on the flanks of Öraefajökull and a fissure within the caldera apply to the maximum expected discharge on a single flank of the volcano in a major eruption.

Table III-5: Melting rates ( $Q_1$  from eq. 4 and  $Q_2$  from eq. 6) and estimated discharge of jökulhlaups (eq. 16) from basaltic fissure eruptions on flanks and fissure eruptions within the caldera.

	<b>Fissure length (m)</b>	<b>ice thickness (m)</b>	<b><math>Q_1</math> (<math>m^3/s</math>)</b>	<b><math>Q_2</math> (<math>m^3/s</math>)</b>	<b><math>Q_T</math> (<math>m^3/s</math>)</b>	<b>Jökulhlaup class</b>
Virkisjökull	3300	80	3,326	4,620	5,775	2
Falljökull	2800	60	2,117	3,920	4,900	2
Grænafjallsgljúfur	2000	80	2,016	2,800	3,500	2
Kotárjökull	2700	80	2,722	3,780	4,725	2
Stigárjökull	3500	80	3,528	4,900	6,125	2
Kvíárjökull	1900	70	1,676	2,660	3,325	2
Steðjakambur-Sléttubjörg	3000	80	3,024	4,200	5,250	2
Caldera - N-S fissure	2200	500	13,860	3,080	17,325	3

Table III-6: Large caldera eruptions, melting rates (eq. 1) and estimated discharge of jökulhlaups (eq. 16) resulting from a rhyolitic, fully subglacial eruption with magma fragmentation.

M' (kg/s)	E' (W)	Q (m <sup>3</sup> /s)	Q <sub>T</sub> (m <sup>3</sup> /s)
1.00E+06	5.6.E+11	1,677	2,300
1.00E+07	5.6.E+12	16,766	23,000
1.00E+08	5.6.E+13	167,665	230,000

$f = 0.7$ ,  $C_g = 1000 \text{ J/(kg } ^\circ\text{C)}$ ,  $\Delta T = 800^\circ\text{C}$

Hypothetical volcanic fissures are oriented radially and the length is dictated by the space available for such a fissure on the ice covered flank. A fissure is not extended onto the lower flanks below ~1000 m elevation, as no geological evidence exists for the presence of such long fissures. The results indicate that jökulhlaups of 3,000–6,000 m<sup>3</sup>/s are possible for flank eruptions during the initial stages as they melt openings in the predominately 60–80 m thick glacier ice on the flanks of Öraefajökull. The size of jökulhlaup does not depend on the size of the outlet glacier, it depends on the length of the volcanic fissure and the ice thickness.

## 6.2. Discharge for eruptions under thick ice in caldera

Three eruption sizes are considered (Table III-6) for the general setting shown in Figure III-10. The smallest eruption magnitude is comparable to the 2010 Eyjafjallajökull eruption (MER =  $1 \cdot 10^6$  kg/s) resulting in melting rates of about 1,700 m<sup>3</sup>/s and a jökulhlaup peak discharge of 2,300 m<sup>3</sup>/s. The second class would correspond to a medium sized sub-Plinian eruption (MER =  $1 \cdot 10^7$  kg/s) and melting rate of about 17,000 m<sup>3</sup>/s and jökulhlaup peak discharge of 23,000 m<sup>3</sup>/s. The largest size considered corresponds to a major Plinian eruption, melting rate of 170,000 m<sup>3</sup>/s and a peak discharge of 230,000 m<sup>3</sup>/s. All of the above scenarios should be regarded as plausible, although the largest event is the most unlikely. An eruption of this magnitude may happen only after a connection has been established to the surface

by melting associated with more modest activity preceding a climactic major Plinian phase. Thus, it may be regarded probable that in a real eruption (such as occurred in 1362), the melting rates never reach the calculated value even though the MER most likely has at some point reached or even exceeded 10<sup>8</sup> kg/s. Moreover, such extremely high melting rates would also be expected to result in meltwater seeking pathways out of the caldera through two or more outlets simultaneously (e.g. Falljökull-Virkisjökull, Kotárjökull and Kviárjökull). The resulting jökulhlaup through each channel would then represent only a part of the total melting. Therefore, the maximum discharge for a jökulhlaup down a particular channel used in modelling is 100,000 m<sup>3</sup>/s.

It should also be clear that the methods applied here do not consider details of hydrograph shape. It is possible that a short lived peak in discharge occurs, that is considerably higher than the calculated melting rates.

## 6.3. Jökulhlaups/lahars resulting from pyroclastic density currents

The results obtained using eq. (11) are presented in Table III-7. The final estimates of Q<sub>T,min</sub> and Q<sub>T,max</sub> are obtained by adding the volume of pyroclastic material to the meltwater volume, assuming that it is a plausible end-member case that most of the material is transported by the meltwater. The fraction of a large PDC assumed to lead to melting varies between catchments. For the largest catchments draining the caldera, Virkisjökull-Falljökull and Kviárjökull, it is assumed that up to 80% of a PDC can flow over these catchments. For Svínafellsjökull it is assumed that an overspill from a PDC principally flowing down Virkisjökull-Falljökull can occur (20% of the PDC) while up to 40% of a large PDC can enter other catchments. Hrutárjökull to the east of Sveinstindur is also included, with a possible 20% of the PDC affecting the catchment. This is an area not considered for flood routing,

but in the event of a large Plinian eruption this sort of event cannot be ruled out.

The results are approximate, and provide only order-of-magnitude estimates, but indicate that lahars of 10,000–20,000 m<sup>3</sup>/s can occur as a result of PDCs. It should also be kept in mind that the values given are averages over 5–10 minutes and the maximum discharge could be higher by a factor of two or so.

Finally, the entrainment of pyroclastic material by meltwater results in high concen-

trations of solids, putting the resulting events firmly in the class of hyper-concentrated flows. The assumption of full entrainment yields a solid mass fraction of about 55%. In reality this value is expected to be somewhat lower. However, entrainment of sediment along the flow path may lead to additional bulking and at least locally, sediment concentrations may be high enough for the flows to behave as debris-flow lahars.

*Table III-7: Melting rates and estimated discharge of lahars caused by pyroclastic density currents (eqs. 11 and 16) resulting from collapse of a plume with mass eruption rate  $\dot{M} = 10^8$  kg/s for  $\tau = 120$  s. Parameters in eq. (11) – min:  $f=0.25$ ,  $\chi=0.25$ ,  $t_{run} = 10$  minutes. – max:  $f=0.7$ ,  $\chi=0.5m$ ,  $t_{run} = 5$  minutes.  $V_w$  is total volume of meltwater,  $V_p = \zeta \dot{M} \rho_p \tau$  is volume of pyroclastic material deposited on glacier.  $V_T$  is the combined volume of meltwater and pyroclasts.*

	Svínafellsjökull	Virkisjökull, Falljökull	Kotárjökull	Steðjaklettur- Sléttubjörg	Hólár- Stígárjökklar	Kvíár- jökull	Hrútár- jökull
$\xi$	0.2	0.8	0.4	0.4	0.4	0.8	0.2
$V_{w,min}$ (m <sup>3</sup> )	$2.5 \times 10^5$	$9.9 \times 10^5$	$4.9 \times 10^5$	$4.9 \times 10^5$	$4.9 \times 10^5$	$9.9 \times 10^5$	$2.5 \times 10^5$
$V_{w,max}$ (m <sup>3</sup> )	$9.9 \times 10^5$	$4.0 \times 10^6$	$2.0 \times 10^6$	$2.0 \times 10^6$	$2.0 \times 10^6$	$4.0 \times 10^6$	$9.9 \times 10^5$
$Q_{min}$ (m <sup>3</sup> /s)	412	1,647	823	823	823	1,647	412
$Q_{max}$ (m <sup>3</sup> /s)	3,293	13,174	6,587	6,587	6,587	13,174	3,293
$V_{p,min}$ (m <sup>3</sup> )	$1.2 \times 10^5$	$4.8 \times 10^5$	$2.4 \times 10^5$	$2.4 \times 10^5$	$2.4 \times 10^5$	$4.8 \times 10^5$	$1.2 \times 10^5$
$V_{p,max}$ (m <sup>3</sup> )	$2.4 \times 10^5$	$9.6 \times 10^5$	$4.8 \times 10^5$	$4.8 \times 10^5$	$4.8 \times 10^5$	$9.6 \times 10^5$	$2.4 \times 10^5$
$V_{T,min}$ (m <sup>3</sup> )	$3.7 \times 10^5$	$1.5 \times 10^6$	$7.3 \times 10^5$	$7.3 \times 10^5$	$7.3 \times 10^5$	$1.5 \times 10^6$	$3.7 \times 10^5$
$V_{T,max}$ (m <sup>3</sup> )	$1.2 \times 10^6$	$5.0 \times 10^6$	$2.5 \times 10^6$	$2.5 \times 10^6$	$2.5 \times 10^6$	$5.0 \times 10^6$	$1.2 \times 10^6$
$Q_{T,min}$ (m <sup>3</sup> /s)	600	2,500	1,200	1,200	1,200	2,500	600
$Q_{T,max}$ (m <sup>3</sup> /s)	4,000	16,700	8,300	8,300	8,300	16,700	4,000

## 7. Conclusions

Models of melting in the cases of caldera eruptions, flank eruptions and pyroclastic density currents during major eruptions have been presented and applied to the catchment areas of Öræfajökull between Svínafellsjökull in the west to Kvíárjökull in the east. The models are simplified semi-empirical approximations constrained by data from known past eruptions. In particular for the PDCs the results can only be regarded as order-of-magnitude estimates.

The results indicate that:

- Eruptions on radial fissures through the shallow ice covering the upper flanks of the volcano should give rise jökulhlaups in the size class 3,000–10,000 m<sup>3</sup>/s.
- The largest caldera eruptions with MERs up to 10<sup>8</sup> kg/s may cause melting rates as high as 200,000 m<sup>3</sup>/s and initiate jökulhlaups with peak discharges up to 260,000 m<sup>3</sup>/s. It is unclear whether a major silicic Plinian eruption would reach such high eruption rates prior to penetration of the glacier. However, jökulhlaups with peak discharges of about 100,000 m<sup>3</sup>/s are considered plausible under present conditions.
- Pyroclastic density currents could generate jökulhlaups with discharges in the range of 10,000–20,000 m<sup>3</sup>/s, which would most likely be hyperconcentrated-flow lahars.

## 8. Acknowledgements

We are grateful to Chris Waythomas for reviewing the chapter. Trausti Jónsson and Tómas Jóhannesson are thanked for proof-reading.

This study was funded by the Icelandic Avalanche Mitigation Fund, the National Power Company, and the Icelandic Road and Coastal Administration.

## 9. References

- Bacon, C. R. (1977). High temperature heat content and heat capacity of silicate glasses: Experimental determination and a model for calculation. *Am. J. Sci.*, 277, 109–135.
- Beverage, J. P., & Culbertson, J. K. (1964). Hyperconcentrations of suspended sediment. *J. Hydraul. Div., Am. Soc. Civ. Eng.*, 90, 117–128.
- Björnsson, H. (1976). Subglacial water reservoirs, jökulhlaups and volcanic eruptions. *Jökull*, 25, 1–15.
- Björnsson, H. (1988). Hydrology of ice caps in volcanic regions. *Soc. Sci. Isl.*, 45, 139, 21 maps.
- Björnsson, H. (2003). Subglacial lakes and jökulhlaups in Iceland. *Global and Planetary Change*, 35, 255–271.
- Björnsson, H., & Pálsson, F. (2008). Icelandic glaciers. *Jökull*, 58, 365–386.
- Branney, M. J., & Kokelaar, P. (2002). *Pyroclastic density currents and the sedimentation of ignimbrites* (Vol. 27). London: Geological Society.
- Bull, K. F., & Buurman, H. (2013). An overview of the eruption of Redoubt Volcano, Alaska. *Journal of Volcanology and Geothermal Research*, 259, 2–15.
- Carey, R. J., Houghton, B. F., & Thordarson, T. (2010). Tephra dispersal and eruption dynamics of wet and dry phases of the 1875 eruption of Askja Volcano, Iceland. *Bull. Volc.*, 72, 259–278.
- Carmichael, I. S., Turner, F. J., & Verhogen, J. (1974). *Igneous Petrology*. New York: McGraw-Hill.
- Degruyter, W., & Bonadonna, C. (2012). Improving on mass flow rate estimates of volcanic eruptions. *Geophys. Res. Lett.*, 39(L16308).
- Dorava, J. M., & Meyer, D. F. (1994). Hydrologic hazards in the lower Drift River basin associated with the 1989–90 eruptions of Redoubt Volcano, Alaska. *Journal of Volcanology and Geothermal Research*, 62, 387–407.
- Edwards, B. R., Gudmundsson, M. T., & Russell, J. K. (2015). Glaciovolcanism. In H. Sigurdsson, B. Houghton, S. R. McNutt, H. Rymer, & J. Stix (Eds.), *Encyclopedia of Volcanoes* (2nd ed., pp. 377–393). Elsevier.
- Einarsson, P. (1991). Umbrotin við Kröflu 1975–1989 (the Krafla episode 1975–1989). In A. Garðarsson, & Á. Einarsson (Eds.), *Náttúra Mývatns* (pp. 321–336). Reykjavík: Hið Íslenska Náttúrufræðifélag.

- Gudmundsson, Á., Óskarsson, N., Grönvold, K., Saemundsson, K., Sigurdsson, O., Stefánsson, R., Gíslason, S. R., Einarsson, P., Brandsdóttir, B., Larsen, G., Jóhannesson, H., and Thordarson, T. (1992). The 1991 eruption of Hekla, Iceland. *Bull. Volc.*, 54, 238–246.
- Gudmundsson, M. T. (2003). Melting of ice by magma-ice-water interactions during subglacial eruptions as an indicator of heat transfer in subaqueous eruptions. In J. D. White, J. L. Smellie, & D. Clague (Eds.), *Explosive Subaqueous Volcanism* (pp. 61–72). Washington D.C.: American Geophysical Union.
- Gudmundsson, M. T. (2005). Subglacial volcanic activity in Iceland. In C. Caseldine, A. Russell, J. Hardardóttir, & Ó. Knudsen (Eds.), *Iceland: Modern processes, Past Environments* (pp. 127–151). Amsterdam: Elsevier.
- Gudmundsson, M. T., & Högnadóttir, Þ. (2005). Ísbráðnun og upptakarennslí jökulhlaupa vegna eldgosa í Eyjafjallajökli og vestanverðum Mýrdalsjökli. (Ice melting and discharge of jökulhlaups due to eruptions in Eyjafjallajökull and the western part of Mýrdalsjökull). In M. T. Gudmundsson, & Á. G. Gylfason (Eds.), *Hættumat vegna eldgosa og hlaupa frá vestanverðum Mýrdalsjökli og Eyjafjallajökli* (pp. 159–180). Reykjavík: Ríkislögreglustjórnin, Háskólaútgáfan.
- Gudmundsson, M. T., & Högnadóttir, Þ. (2006). Ísbráðnun og upptakarennslí jökulhlaupa vegna eldgosa í Kötluöskju og austanverðum Mýrdalsjökli. Reykjavík: Jarðvísindastofnun Há-skólans.
- Gudmundsson, M. T., Högnadóttir, Þ., Kristinsson, A. B., & Gudbjörnsson, S. (2007). Geothermal activity in the subglacial Katla caldera, Iceland, 1999–2005, studied with radar altimetry. *Annals of Glaciology*, 45, 66–72.
- Gudmundsson, M. T., Sigmundsson, F., & Björnsson, H. (1997). Ice-volcano interaction of the 1996 Gjalp subglacial eruption, Vatnajökull, Iceland. *Nature*, 389, 954–957.
- Gudmundsson, M. T., Sigmundsson, F., Björnsson, H., & Högnadóttir, Þ. (2004). The 1996 eruption at Gjalp, Vatnajökull ice cap, Iceland: efficiency of heat transfer, ice deformation and subglacial water pressure. *Bulletin of Volcanology*, 66, 46–65.
- Gudmundsson, M. T., Thordarson, T., Höskuldsson, Á., Larsen, G., Björnsson, H., Prata, F. J., Oddsson, B., Magnússon E., Högnadóttir, T., Petersen, G. N., Hayward, C. L., Stevenson, J. A., and Jónsdóttir, I. (2012). Ash generation and distribution from the April–May 2010 eruption of Eyjafjallajökull, Iceland. *Scientific Reports*, 2(572).
- Gudmundsson, M., & Larsen, G. (2013). Jökulhlaup. In J. Sólnes, F. Sigmundsson, & B. Bessason (Eds.), *Náttúruvá á Íslandi. Eldgos og Jarðskjálftar* (pp. 156–170). Reykjavík: Viðlagatrygging Íslands, Háskólaútgáfan.
- Hákonardóttir, K. M., Jóhannesson, T., & Sampl, P. (2005). Líkanreikningar á jökulhlaupum niður suðurhliðar Eyjafjallajökuls (Hydraulic simulations of glacial outbursts on the southern slopes of Eyjafjallajökull). In M. T. Gudmundsson, & Á. G. Gylfason (Eds.), *Hættumat vegna eldgosa og hlaupa frá vestanverðum Mýrdalsjökli og Eyjafjallajökli (Hazard assessment of volcanic eruptions and glacial outbursts for Eyjafjallajökull and the western outwash plain of Mýrdalsjökull)* (pp. 181–196). Reykjavík: Ríkislögreglustjórnin, Háskólaútgáfan.
- Helgadóttir, Á., Pagneux, E., Roberts, M. J., Jensen, E. H., & Gíslason, E. (2015). Örafajökull Volcano: Numerical simulations of eruption-induced jökulhlaups using the SAMOS flow model. In E. Pagneux, M. T. Gudmundsson, S. Karlsdóttir, & M. J. Roberts (Eds.), *Volcanogenic floods in Iceland: An assessment of hazards and risks at Örafajökull and on the Markarfljót outwash plain* (pp. 73–100). Reykjavík: IMO, IES-UI, NCIP-DCPEM.
- Hólm, S. L., & Kjaran, S. P. (2005). Reiknilíkan fyrir útbreiðslu hlaupa úr Entujökli (Hydraulic model of floods from Entujökull). In M. T. Gudmundsson, & Á. G. Gylfason (Eds.), *Hættumat vegna eldgosa og hlaupa frá vestanverðum Mýrdalsjökli og Eyjafjallajökli (Hazard assessment of volcanic eruptions and glacial outbursts for Eyjafjallajökull and the western outwash plain of Mýrdalsjökull)* (pp. 197–210). Reykjavík: National Commissioner of Police.
- Hreinsdóttir, S., Sigmundsson, F., Roberts, M. J., Björnsson, H., Grapenthin, R., Arason, P., Arnadóttir, T., Hólmjárn, J., Geirsson, H., Bennett, R. A., Gudmundsson, M. T., Oddsson, B., Ófeigsson, B. G., Villemin, T., Jónsson, T., Sturkell, E., Höskuldsson, Á., Thordarson, T., and Óladóttir, B. A. (2014). Volcanic plume height correlated with magma pressure change at Grímsvötn Volcano, Iceland. *Nature Geoscience*, 7, 214–218.
- Höskuldsson, Á., & Sparks, R. S. (1997). Thermodynamics and fluid dynamics of effusive subglacial eruptions. *Bull. Volcanol.*, 59, 219–230.
- Jarosch, A. H., Gudmundsson, M. T., Högnadóttir, T., & Axelsson, G. (2008). The progressive cooling of the hyaloclastite ridge at Gjalp, Iceland, 1996–2005. *Journal of Volcanology and Geothermal Research*, 170, 218–219.

- Jude-Eton, T. C., Thordarson, T., Gudmundsson, M. T., & Oddsson, B. (2012). Dynamics, stratigraphy and proximal dispersal of supraglacial tephra during the ice-confined 2004 eruption at Grímsvötn volcano, Iceland. *Bull. Volc.*, *74*, 1057–1082.
- Larsen, G. (2000). Holocene eruptions within the Katla volcanic system, south Iceland: Characteristics and environmental impact. *Jökull*, *49*, 1–28.
- Larsen, G., Guðmundsson, M. T., & Sigmarsson, O. (2013). Katla. In J. Sólnes, F. Sigmundsson, & B. Bessason (Eds.), *Náttúruvá á Íslandi. Eldgos og Jarðskjálftar* (pp. 211–233). Reykjavík: Viðlagatrygging Íslands/Háskólaútgáfan.
- Larsen, G., Vilmundardóttir, E., & Þorkelsson, B. (1992). Heklugosið 1991: Gjóskufallið og gjóskulagið frá fyrsta degi gossins. (Hekla eruption of 1991: Fallout of tephra on first day of eruption). *Náttúrufræðingurinn*, *61*, 159–176.
- Magnússon, E., Gudmundsson, M. T., Sigurdsson, G., Roberts, M. J., Höskuldsson, F., & Oddsson, B. (2012a). Ice-volcano interactions during the 2010 Eyjafjallajökull eruption, as revealed by airborne radar. *J. Geophys. Res.*, *117*, B07405.
- Magnússon, E., Pálsson, F., Björnsson, H., & Gudmundsson, S. (2012b). Removing the ice cap of Oraefajökull central volcano, SE-Iceland: Mapping and interpretation of bedrock topography, ice volumes, subglacial troughs and implications for hazards assessments. *Jökull*, *62*, 131–150.
- Mandeville, C. W., Carey, S., Sigurdsson, H., & King, J. (1994). Areomagnetic evidence for high-temperature emplacement of the 1883 subaqueous pyroclastic flows from Krakatau Volcano, Indonesia. *Journal of Geophysical Research*, *99*(B5), 9487–9504.
- Mastin, L. G., Guffanti, M., Servranckx, R., Webley, P., Barsotti, S., Dean, K., . . . Waythomas, C. F. (2009). A multidisciplinary effort to assign realistic source parameters to models of volcanic ash-cloud transport and dispersion during eruptions. *Journal of Volcanology and Geothermal Research*, *186*(1–2), 10–21.
- Oddsson, B., Gudmundsson, M. T., Larsen, G., & Karlsdóttir, S. (2012). Monitoring the plume from the basaltic phreatomagmatic 2004 Grímsvötn eruption — application of weather radar and comparison with plume models. *Bull. Volc.*, *74*, 1395–1407.
- Pierson, T. C., editor. (1999). *Hydrologic consequences of hot-rock/snowpack interactions at Mount St. Helens Volcano, Washington 1982–84*. Denver: U.S. Dept. of the Interior, U.S. Geological Survey Information Services.
- Pierson, T. C., Janda, R. J., Thouret, J. C., & Borrero, C. A. (1990). Perturbation and melting of snow and ice by the 13 November 1985 eruption of Nevado del Ruiz, Columbia, and consequent mobilization, flow and deposition of lahars. *Journal of Volcanology and Geothermal Research*, *41*, 17–66.
- Roberts, M. J., & Gudmundsson, M. T. (2015). Öraefajökull Volcano: Geology and historical floods. In E. Pagneux, M. T. Gudmundsson, S. Karlsdóttir, & M. J. Roberts (Eds.), *Volcanogenic floods in Iceland: An assessment of hazards and risks at Öraefajökull and on the Markarfljót outwash plain* (pp. 17–44). Reykjavík: IMO, IES-UI, NCIP-DCPEM.
- Roche, O., Phillips, J., & Kelfoun, K. (2013). Pyroclastic density currents. In S. A. Fagents, T. K. Gregg, & R. M. Lopes (Eds.), *Modeling volcanic processes* (pp. 203–229). Cambridge University Press.
- Schmid, A., Sonder, I., Seegelken, R., Zimanowski, B., Büttner, R., Gudmundsson, M. T., & Oddsson, B. (2010). Experiments on the heat discharge at the dynamic magma-water-interface. *Geophys. Res. Lett.*, *37*, L20311.
- Scott, A. C., & Glasspool, I. (2004). Charcoal reflectance as a proxy for the emplacement temperature of pyroclastic flow deposits. *Geology*, *33*, 589–592.
- Siebert, L., Cottrell, E., Venske, E., & Andrews, B. (2015). Earth's volcanoes and their eruptions: An overview. In H. Sigurdsson, B. Houghton, S. R. McNutt, H. Rymer, & J. Stix (Eds.), *Encyclopedia of Volcanoes* (2nd ed., pp. 239–255). Elsevier.
- Smellie, J. L. (2002). The 1969 subglacial eruption on Deception Island (Antarctica): events and processes during an eruption beneath a thin glacier and implications for volcanic hazards. In J. L. Smellie, & M. Chapman (Eds.), *Ice-volcano interaction on Earth and Mars* (pp. 59–80). London: Geological Society.
- Sparks, R., Bursik, M., Carey, S., Gilbert, J., Glaze, L., Sigurdsson, H., & Woods, A. (1997). *Volcanic Plumes*. Chichester: John Wiley and Sons.
- Thorarinsson, S. (1958). The Öraefajökull eruption of 1362. *Acta Naturalia Islandica*, *2*(4), 100.
- Thorarinsson, S. (1967). The eruption of Hekla in historic times. A tephrocronological study. In *The eruption of Hekla 1947–48*. Reykjavík: Societas Scientiarum Islandica.
- Thordarson, T., & Self, S. (1993). The Laki (Skaftár Fires) and Grímsvötn eruptions in 1783–1785. *Bull. Volc.*, *55*, 233–263.

- Tómasson, H. (1996). The Jökulhlaup from Katla in 1918. *Annals of Glaciology*, 22, 249-254.
- Trabant, D., Waitt, R. B., & Major, J. J. (1994). Disruption of Drift glacier and origin of floods during the 1989–1990 eruptions of Redoubt Volcano, Alaska. *Journal of Volcanology and Geothermal Research*, 62, 369–385.
- Waitt, R., Pierson, T. C., Macleod, N. S., Janda, R. J., Voight, B., & Holcomb, R. T. (1983). Eruption-triggered avalanche, flood and lahar at Mount St. Helens – effects of winter snowpack. *Science*, 221, 1394–1397.
- Walder, J. S. (1999). Nature of depositional contacts between pyroclastic deposits and snow and ice. In T. Pierson (Ed.), *Hydrologic consequences of hot-rock/snowpack interactions at Mount St. Helens Volcano, Washington 1982–1984* (pp. 9–18). Denver: U.S. Dept. of the Interior, U.S. Geological Survey Information Services.
- Walder, J. S. (2000). Pyroclast/snow interactions and thermally driven slurry formation. Part 1: theory for monodisperse grain beds. *Bulletin of Volcanology*, 62, 105–118.
- Walder, J. S. (2000). Pyroclast/snow interactions and thermally driven slurry formation. Part 2: experiments and theoretical extension to polydisperse tephra. *Bulletin of Volcanology*, 62, 119–129.
- Waythomas, C. F., Pierson, T. C., Major, J. J., & Scott, W. E. (2013). Voluminous ice-rich and water rich lahars generated during the 2009 eruption of Redoubt Volcano, Alaska. *Journal Volc. Geoth. Res.*, 259, 389–413.
- Wohletz, K., Zimanowski, B., & Büttner, R. (2013). Magma-water interactions. In S. A. Fagents, T. K. Gregg, & R. M. Lopes (Eds.), *Modeling Volcanic Processes* (pp. 230–254). Cambridge University Press.
- Woodcock, D. C., Lane, S. J., & Gilbert, J. S. (2012). Particle-water heat transfer during explosive eruptions. *J. Geop. Res. Solid Earth*, 117, B10205. doi:10.1029/2012JB009240
- Woodcock, D. C., Lane, S. J., & Gilbert, J. S. (2014). Ice-melt rates in liquid-filled cavities during explosive subglacial eruptions. *J. Geop. Res. Solid Earth*, 119, 1803–1817.
- Woodhouse, M. J., Hogg, A. J., Phillips, J. C., & Sparks, R. S. (2013). Interaction between volcanic plumes and wind during the 2010 Eyjafjallajökull eruption, Iceland. *J. Geophys. Res.*, 118, 92–109.
- Zimanowski, B. (1998). Phreatomagmatic explosions. In A. Freundt, & M. Rosi (Eds.), *From Magma to Tephra: Modelling Physical Processes of Explosive Volcanic Eruptions* (pp. 25–54). Elsevier.
- Zimanowski, B., & Büttner, R. (2003). Phreatomagmatic explosions in subaqueous eruptions, in Explosive Subaqueous Volcanism. In J. D. White, J. L. Smellie, & Clague, D. A. (Eds.), *Explosive Subaqueous Volcanism* (pp. 51-60). Washington D.C.: American Geophysical Union.